Assimilating multivariate remote sensing data into a fully coupled subsurface-land surface hydrological model

Samira Sadat Soltani, Behzad Ataie-Ashtiani, Ahmad Al Bitar, Craig.T. Simmons, Anis A. Younes, Marwan Fahs

Assimilating multivariate remote sensing data into a fully coupled subsurface-land surface hydrological model

Samira Sadat Soltani [a, b], Behzad Ataie-Ashtiani [a,c], Ahmad Al Bitar [d], Craig.T. Simmons[e], Anis Younes[b]; Marwan Fahs[*b]

[a] *Department of Civil Engineering, Sharif University of Technology, Tehran, Iran*
[b] *Institut Terre et Environnement de Strasbourg, Université de Strasbourg, CNRS, ENGEES, UMR 7063, 67084 Strasbourg, France*
[c] *School of Environmental and Life Sciences, The University of Newcastle, Callaghan, New South Wales, Australia*
[d] *CESBIO, Université de Toulouse, CNES, CNRS, IRD, INRAe, UPS, 18 avenue Edouard Belin, 31401 Toulouse, France*
[e] *College of Engineering, Science and Environment, The University of Newcastle, Newcastle, Australia*

[*]Corresponding author

Marwan Fahs (0000-0003-0454-6476)- ORCID;

Email: fahs@unistra.fr

Samira Sadat Soltani (0000-0002-1111-1385) – ORCID;

Behzad Ataie-Ashtiani (0000-0002-1339-3734)- ORCID;

Ahmad Al Bitar (0000-0002-1756-1096)-ORCID;

Craig T. Simmons (0000-0001-5399-6292)- ORCID;

Anis Younes (0000-0002-6004-7033)- ORCID;

Abstract

Hydrological models play a crucial role in tracking and predicting terrestrial water storage, yet they face challenges due to uncertainties and inaccuracies caused by various factors such as meteorological processes and data limitations. To refine these models, data assimilation has emerged as a valuable tool, utilizing a new source of data to update model states while considering associated uncertainties, thereby enhancing our comprehension and predictive capabilities in hydrological processes. In this context, satellite data are receiving increasing attention because they can cover large areas and are useful in detecting spatial and temporal variability of water.

In most existing studies related to satellite data assimilation in hydrological models, one source satellite data is used in the analysis. This study focuses on improving subsurface water storage model accuracy by assimilating data from different satellite sources. In particular, we used data from the Soil Moisture and Ocean Salinity (SMOS) satellite and terrestrial water storage data from the Gravity Recovery and Climate Experiment (GRACE). The data are assimilated into a fully coupled subsurface-surface hydrological model, developed with ParFlow-CLM (PARallel FLOW- Community Land Model). The investigation is conducted in Iran. Employing an Ensemble Kalman Filter, three assimilation scenarios are explored: (i) GRACE, (ii) SMOS, and (iii) the combined assimilation of both GRACE and SMOS data (joint). Findings are validated

against the Soil Moisture Active Passive (SMAP) and in-situ groundwater data by using a novel probabilistic reliability framework, demonstrating the advantages of joint data assimilation.

The study highlights the influence of assimilated remote sensing data type on the effectiveness of data assimilation. Assimilating GRACE data enhances groundwater level estimations. However, SMOS data positively impacts topsoil moisture estimations, but adversely affects groundwater level estimates. Importantly, the assimilation of both GRACE and SMOS data through multivariate (joint) data assimilation significantly improves accuracy for both soil moisture estimation and groundwater level estimation.

Keywords: Hydrological Modeling, ParFlow-CLM, Multivariate Data Assimilation, Ensemble Kalman Filter, Groundwater, Soil Moisture

1 Introduction

Accurate hydrologic simulations are essential for managing water resources, predicting future water availability, and anticipating extreme events. For understanding the impacts of climate change and water resource availability, estimation of terrestrial water storage (TWS) components (e.g., soil moisture, groundwater storage, snow, surface water) is essential for understanding the impacts of climate change and water resource availability (Hirschi et al., 2007; Soltani et al., 2021). Soil moisture is the degree of saturation of an unsaturated soil. It is equal to 1 when the soil is saturated and 0 when the soil is dry. Groundwater storage is is the volume of water stored in the aquifer (saturated zone). Each TWS component has a particular impact on the climate as a whole and it is also an important climate change driver (Bierkens and Van den Hurk, 2007; Green et al., 2011). For instance, a major source of atmospheric humidity is supplied by soil moisture, and it is therefore a strong contributor to the climate system (Seneviratne et al., 2010). In order to obtain accurate seasonal forecasts, soil moisture should be accurately predicted (Koster et al., 2010; Van den Hurk et al., 2012). Groundwater storage variations (ΔGWS) should be determined accurately to be able to assess water resources in a reliable fashion, especially for dry climates with large abstractions of groundwater and significant temporal and spatial of climate variability (Soltani et al., 2022a).

Despite the importance of having reliable estimates of TWS, knowledge of spatial and temporal variations in TWS and its components is generally lacking. This is particularly true at large

77 scales, or in less-developed countries where there is, in general, an absence of global monitoring
78 systems (Soltani et al., 2020).

79 Ground-based measurements, while very accurate, only provide point-wise estimates (Dorigo
80 et al., 2011; Soltani et al., 2020). This is where hydrological models stand out as a solution to
81 fill this gap at high spatiotemporal resolutions (e.g., Döll et al., 2003; Van Dijk, 2010). As a
82 result, hydrological models are essential tools for sustainable management of water resources
83 (Yu et al., 2015). However, absence of reliable data often means that the modeling process is
84 challenged and this is further compounded by errors in modeling and model parameter
85 uncertainties (Van Dijk et al., 2011; Vrugt et al., 2013). As a result, simulation results can be
86 unreliable. Subsequently, models can be made more trustworthy by data assimilation (DA)
87 (Bertino et al., 2003). For this purpose, additional information is supplied by means of new
88 datasets which can constrain the estimators of model's states to more meaningful values
89 (Bertino et al., 2003; Hoteit et al., 2012).

90 Assimilation of satellite data has applications in various fields such as magnetospheric (Garner
91 et al., 1999), ocean (Bennett, 2005; Lahoz et al., 2007) and atmosphere (Schunk et al., 2004;
92 Altaf et al., 2014) studies. It is also predominantly used in hydrological models where the
93 accuracy of flux and/or storage components needs to be enhanced (e.g., Dillon et al., 2016;
94 Khaki et al., 2018a; Khaki et al., 2018b).

TWS variations (ΔTWS) can be derived from gravity measurements by the Gravity Recovery And Climate Experiment (GRACE) satellite mission (Tapley et al., 2004) and have been used in data assimilation studies and discussed widely in the literature (Soltani et al., 2021). Soltani et al. (2021) provided an in-depth review of the recent studies on incorporating GRACE TWS data into hydrological models, highlighting their limitations, problems, and progress. They also presented an overview of the advantages and limitations of various data assimilation techniques, with a focus on the capacity of sequential methods for hydrological applications. Various filtering techniques, such as variational methods and sequential filtering, have been proposed and developed across different fields to achieve DA objectives. In recent decades, there has been significant attention on GRACE DA, particularly for improving deep storage components like groundwater levels (Tangdamrongsub et al., 2015; Zaitchik et al., 2008; Soltani et al., 2021). While the benefits of GRACE DA are evident in deep storage, its effectiveness in enhancing surface soil moisture remains a challenge (Li et al., 2012; Tangdamrongsub et al., 2017; Tian et al., 2017).

The goal of multivariate DA is to combine the strengths of SM DA and GRACE DA to simultaneously improve soil moisture and groundwater level estimates. Recent studies showed that the accuracy of surface and deep storage components could be improved by assimilating GRACE and soil moisture data (Tian et al., 2017; Tangdamrongsub et al., 2020). Furthermore, and used multivariate DA to increase the skills of model state estimations and climate

114 assessment indicators utilizing several satellite soil moisture and snow products (Jasinski et al.,
115 2019). Based on these results, multivariate assimilation of GRACE and satellite soil moisture
116 data (e.g., SMOS (Soil Moisture and Ocean Salinity)) is projected to improve soil moisture and
117 groundwater estimates (Kumar et al., 2019).

118 This study develops a multivariate DA with GRACE and SMOS data to improve the accuracy
119 of regional soil moisture and groundwater level estimates. The main research objective is to
120 investigate the performance of multivariate DA in simultaneously improving soil moisture and
121 groundwater level estimates. Different DA schemes are developed to incorporate different
122 observations into the DA system simultaneously. Three different DA scenarios subject to three
123 different observation cases (SM-only, GRACE-only, and both) are evaluated by using a novel
124 probabilistic framework.

125 The hydrological model used in this study is the fully coupled surface-subsurface hydrological
126 model ParFlow-CLM (PARallel FLOW- Community Land Model), known for simulating the
127 intricate interactions between land surface and subsurface hydrology effectively. This
128 specialized model is particularly tailored to accurately represent the dynamics of water and
129 energy fluxes at high spatial resolutions across extensive geographical areas (Sulis et al., 2017).
130 ParFlow is a grid-based parallel integrated two-way coupled hydrologic modeling technique
131 through which the surface and subsurface flow is simulated simultaneously in 3D. The ParFlow
132 model can be used for various surface and groundwater problems over large and small basins

(Ferguson and Maxwell, 2012). It does not include surface processes such as evaporation. Therefore, to generate more realistic outputs, ParFlow is often coupled with a land surface model, in particular, CLM (Kollet and Maxwell, 2008). The coupled ParFlow-CLM model combines high-resolution simulations, complex terrain representation, vegetation dynamics, climate change and land use studies, water resources management, and flood and drought analysis. ParFlow has been used to study different surface and groundwater problems in large domains (Ferguson and Maxwell, 2012), small basins (Kollet and Maxwell, 2006), and even subsurface–surface (Soltani et al., 2022b) and atmospheric (Shrestha et al., 2014) coupling.

2 Case study description

The case study area encompasses portions of the Persian Gulf and the Sea of Oman basin, notably including several significant sub-basins in the western and southwestern regions of Iran. This area incorporates the Karun, Jarahi, and Karkheh sub-basins, and collectively covers a substantial expanse of 158,000 km^2. This territory constitutes approximately ten percent of Iran's total land area. This case study is bounded by [29°N 35° N] and [46° E and 53° E], in the west of Iran and important cities such as Ahvaz, Khorramshahr, Shahr-e Kord, Kermanshah and Yasuj are in this region (Figure 1). In the mountainous regions, the elevation ranges from over 4,000 m to sea level at the Persian Gulf coast (Figure 1).

Precipitation varies seasonally and geographically owing to the passage of mid-latitude storms that originate in the Mediterranean Sea region and the effects of the complicated topography (Kiany et al., 2020) The study area's mean annual precipitation ranges from 100 mm in the plains in the southwest to >900 mm in some of the eastern mountainous regions (Raziei et al., 2012) and the average temperature in the summer and winter are 48° and 4°C. Deserts in this zone have an area of 1.3×10^4 km^2, which is equal to eight percent of the basin's area, which are predominantly located in the south and southwest arid and hyper-arid climatic zones (Ardebili and Khademalrasoulb, 2018).

The important rivers that run through this basin are Jarahi, Karkheh, Karun, Zohreh and Dez, supplying 34×10^9 m^3 of water annually, which is about 33% contribution of the total water resources of the entire country. 83% contribution of the water consumption in Zohreh-Jarahi, 88% in Karun and 89% in Karkheh were by agricultural use (Rahmani, 2021). This basin is a hub for agriculture, with 26.2% dedicated to crops such as rice, wheat, barley, cotton, corn, sugarcane, and various summer crops, and 12% dedicated to tree cultivation. These crops thrive on the fertile plains of the southwest, nourished by the water from the five major rivers (Ardebili and Khademalrasoulb, 2018).

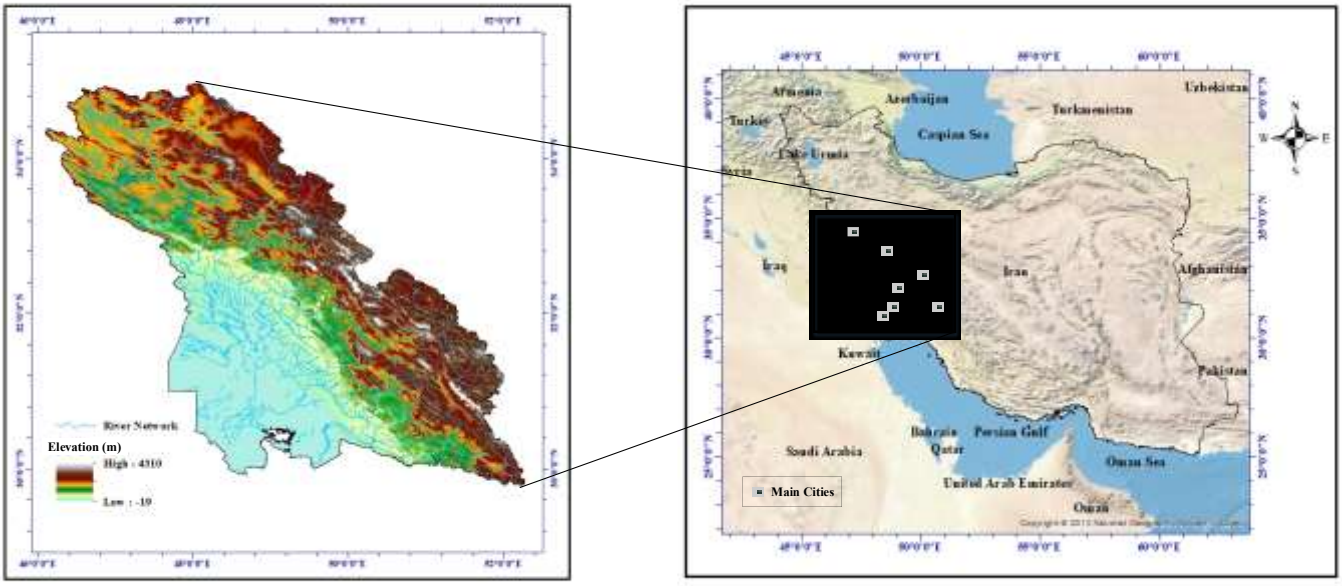

166

167 **Figure 1.** The geographical location of the case study, located in west and southwest of Iran,
168 overlaid by the study location Digital Elevation Model (DEM) and the river network.

169 ## 3 Methodology and data

170 ### 3.1 Model description

171 The ParFlow-CLM model comprises two essential components. First, the ParFlow model solves
172 the Richards equation, a governing equation for water flow through 3-D variably saturated
173 porous media (Ashby and Falgout, 1996; Kollet and Maxwell, 2006). The Richards equation
174 takes into account critical factors such as soil properties, and topography, allowing the
175 simulation of subsurface water movement. The ParFlow model utilizes a finite difference

176 approach and parallel computing techniques to efficiently handle the complex computations
177 involved in modeling these intricate processes (Kollet and Maxwell, 2006).

178 Second component , CLM (Oleson et al., 2004, 2008) focuses on representing land surface
179 processes. It consists of modules dedicated to surface energy balance, vegetation dynamics,
180 biogeochemistry, and snow accumulation and melt. These modules interact with the ParFlow
181 subsurface component through flux exchanges, enabling processes such as water infiltration
182 from the surface to the subsurface, evapotranspiration from vegetation, and heat transfer
183 between the land surface and subsurface to be effectively simulated and integrated into the
184 model (Soltani et al., 2022c). In the sequential information exchange procedure, ParFlow sends
185 the updated relative saturation (S_w) and pressure (ψ) for the top 10 layers to CLM. In turn, CLM
186 sends the depth differentiated source and sink terms for soil moisture [top soil moisture flux
187 (qrain), soil evapotranspiration (qe)] for the top 10 soil layers to ParFlow (Shrestha et al., 2014).
188 For more details on the numerical aspects and other features of the model, refer to Kollet and
189 Maxwell (2006). Additionally, the model's structure and configuration are visually represented
190 in Figure 2.

191 The critical soil hydraulic properties, such as water retention and hydraulic conductivity curves,
192 are described using Mualem-van Genuchten functions (Van Genuchten, 1980), with their
193 parameters estimated through the application of pedotransfer functions. Notably, leveraging
194 physics-based Integrated Hydrological Models (IHMs) offers a significant advantage over

lumped hydrological models. IHMs deliver robust results without requiring extensive calibration steps (Poméon et al., 2020).

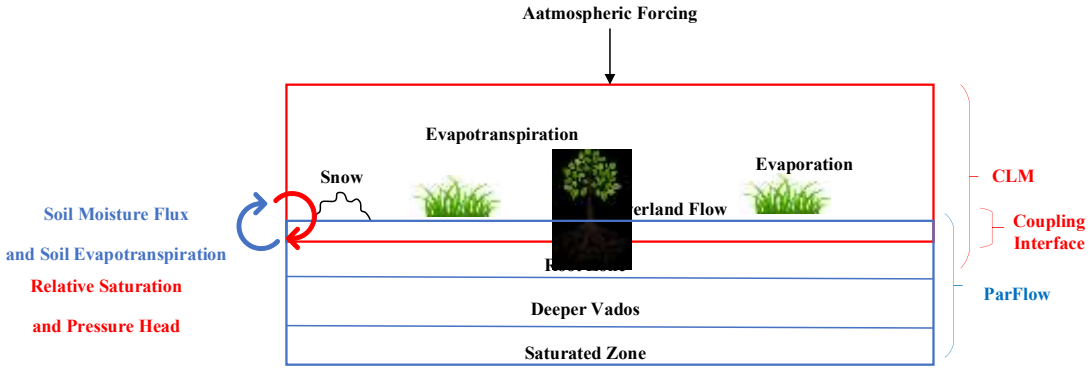

Figure 2. Schematic of ParFlow-CLM model

The Van Genuchten relationships are utilized to define the relative saturation and permeability functions as follows:

$$S_w(\psi_p) = \frac{s_{sat} - s_{res}}{(1+(\alpha\psi_p)^n)^{(1-1/n)}} + s_{res} \quad (1)$$

$$K_r(\psi_p) = \frac{(1-\frac{(\alpha\psi_p)^{n-1}}{(1+(\alpha\psi_p)^n)^{(1-1/n)}})^2}{(1+(\alpha\psi_p)^n)^{\frac{(1-1/n)}{2}}} \quad (2)$$

where s_{sat} [–] is the relative saturated water content, s_{res} [–] is the relative residual saturation, α [L^{-1}] and n [–] are soil parameters.

3.2 Water balance

ParFlow can perform water balance calculations for the Richards' equation, overland flow, and CLM capabilities. There are two types of water balance storage: subsurface and surface, as well

as two types of flux calculations: overland flow and evapotranspiration. The storage components are measured in units [L^3], whereas the fluxes can be instantaneous and measured in units [L^3T^{-1}] or cumulative over an output interval and measured in units [L^3]. The water balance has the following form (Maxwell et al., 2016):

$$\frac{\Delta[Vol_{surface} + Vol_{subsurface}]}{\Delta t} = Q_{overland} + Q_{evapotranspiration} + Q_{source/\sin k} \quad (3)$$

where $Vol_{subsurface}$ is the subsurface storage [L^3], $Vol_{surface}$ is the surface storage [L^3], $Q_{overland}$ is the overland flux [L^3T^{-1}], $Q_{evapotranspiration}$ is the evapotranspiration flux passed from CLM [L^3T^{-1}], and $Q_{sourc/esink}$ are any other source or sink fluxes specified in the simulation [L^3T^{-1}]. Only the external fluxes passed from CLM are included in $Q_{evapotranspiration}$, which needs to be recorded as a variable in ParFlow. It is important to note that these volume and flux quantities, like any other quantity in ParFlow, are computed spatially across the entire domain and returned as array values. The subsurface water is the summation of soil moisture and groundwater storage. It is represented by the subsurface equivalent water thickness which is computed for all active cells in the domain, as follows (the outcomes represent as an array of balances by domain) (Maxwell et al., 2016):

$$H_{subsurface} = \sum_{\Omega} [S_w(\psi_p) \times S_s \times \psi_p + S_w(\psi_p) \times \psi_p] \quad (4)$$

Here, $H_{subsurface}$ [L] is equivalent water thickness in subsurface and S_s [-] is the specific storage. The surface equivalent water thickness ($H_{surface}$)is determined using the continuity equation over the top surface boundary cells in the domain Γ ,as obtained by the mask. This is done on a cell-by-cell basis (resulting in an array of balances across the domain) like follows (Maxwell et al., 2016):

$$H_{surface} = \sum_{\Gamma} \psi_p \tag{5}$$

The summation of surface equivalent water thickness and subsurface equivalent water thickness results in TWS derived by GRACE.

3.2 Data

3.2.1 Land surface data and atmospheric forcing

The land surface input data include topography, land cover, soil characteristics, and physiological parameters of the canopy which are static variables. Global Multiresolution Terrain Elevation Data 2010 (Danielson et al., 2011) was used as Digital Elevation Model (DEM) which has a resolution of 1km (see Figure 1). The Moderate Resolution Imaging Spectroradiometer (MODIS) satellite land-use classification (Friedl et al., 2002) was also used, where it was converted to Plant Functional Types (PFT). In order to include the soil characteristics, the percentage of soil and clay were obtained using FAO/UNESCO Digital Soil Map of the World (Batjes, 1997) which has numerous soil classes consisting of 19 classes,

242 which was based on Schaap and Leij (1998)'s pedotransfer functions. For the Manning's
243 coefficient, the values which has been proposed based on relationship between landcover type
244 and roughness is used (Asante et al., 2008).

245 The atmospheric forcing of the coupled ParFlow model with CLM including barometric
246 pressure, wind speed, precipitation, specific humidity, downward shortwave and longwave
247 radiations and air temperature near the surface is provided from GLDAS-Noah Land Surface
248 Model L4 V2.1 data (https://disc.gsfc.nasa.gov/datasets/GLDAS_NOAH025_3H_2.1). This
249 has a spatial resolution of 0.25° and temporal resolution of 3-hourly (due to the temporal
250 resolution of the GLDAS data), and the data used covers the time period of 2015-2020. All
251 model inputs given in **Table 1**, were re-projected to have an equal cell size of 0.25° resolution.
252 In this study, the model was employed for a total thickness of 300 m over 100 model layers
253 ($n_{Z=}$100) with different thickness. The model was implemented with a horizontal resolution of
254 0.25°. This grid comprises 28 cells in the x-direction (nx=28) and 24 cells in the y-direction
255 (ny=24) (see Figure 3).

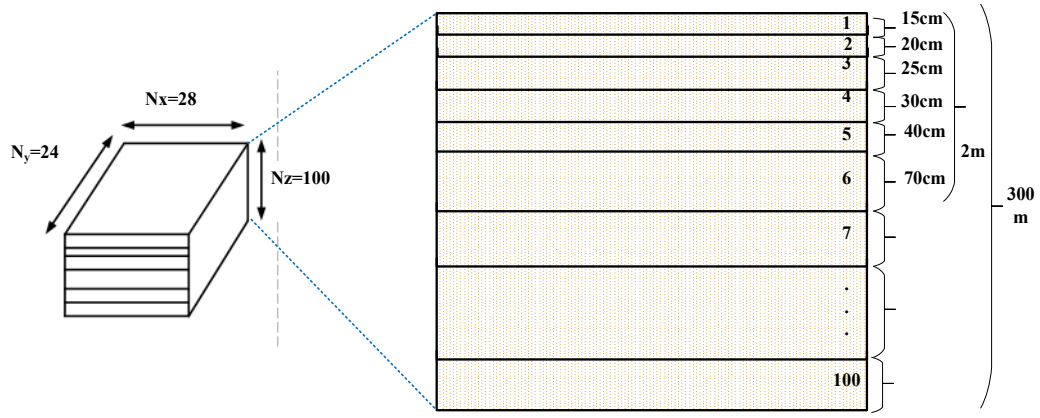

256

257 **Figure 3.** Visualization of the domain dimensions

258 ### 3.2.2 GRACE TWS

259 The GRACE data release 05 (RL05) was supplied by the University of Texas at Austin's Center
260 for Space Research (CSR) (Bettadpur, 2012). This release includes the monthly spherical
261 harmonic coefficients (SHC) complete up to degree and order 96. The GRACE-derived TWS,
262 as well as its uncertainty over the case study, are calculated as follows: First, the Swenson et al.
263 (2008) degree 1 coefficients (SHC) are restored, and the C20 term is replaced by the value
264 derived from the satellite laser range (Cheng and Tapley, 2004). Second, the mean covering the
265 period from March 2015 to June 2017 is calculated and subtracted from the monthly product to
266 produce the SHC variations, then restriping (Swenson and Wahr, 2006) and 300-km radius
267 Gaussian smoothing filters are applied to the SHC variations to reduce the high-frequency noise.
268 Third, following the method outlined by Wahr et al. (1998), the TWS variation (TWS) is

computed from the filtered SHC variations. Finally, a signal restoration algorithm (e.g., Chen et al., 2014) is used to the computed TWS. The strategy iteratively searches for the true TWS using a forward model built entirely from GRACE data. To be consistent with the model estimate, the ParFlow-CLM estimates of TWS temporal mean value (March 2015–June 2017) is added to the GRACE-derived TWS to produce the absolute TWS prior to the assimilation procedure (Zaitchik et al., 2008).

3.2.3 SMOS and SMAP soil moisture datasets

This research relies on daily satellite soil moisture retrievals from the Soil Moisture and Ocean Salinity mission (SMOS, Kerr et al., 2012). The SMOS missions consist in a L-Band (1.4 Ghz) interferometric radiometer that is sensible to surface soil moisture and vegetation optical thickness over continental surfaces. The level 3 gridded product (Al Bitar et al., 2017) provided by the Centre Aval de Traitement des Données SMOS (CATDS, https://www.catds.fr) and run by the French Research Institute for Exploitation of the Sea for the Centre National d'Etudes Spatiales (CNES) is used to collect SMOS data (IFREMER). On the Equal-Area Scalable Earth (EASE; Brodzik et al., 2012) grid, data are accessible from January 2010 to present, with a spatial resolution of 25 km in m^3/m^3. SMOS data with a daily temporal resolution are spatially rescaled from 25 km×25 km to 0.25°×0.25° resolution using the nearest neighbor interpolation to match ParFlow-CLM. The data is filtered for Radio Frequency Interference (RFI) using the RFI probability flag. Jamei et al. (2022) have evaluated the accuracy of soil moisture derived

288 by SMOS (SM_{SMOS}) products over the Southwest and West regions of Iran for the time period
289 of 2012-2015. The research results demonstrate that SM_{SMOS} model exhibits a high level of
290 accuracy and agreement when compared to in-situ measurements. These findings substantiate
291 the efficacy of utilizing remotely sensed data for estimating soil moisture, highlighting the
292 potential of SM_{SMOS} as a reliable tool in such applications.

293 The Soil Moisture Active Passive (SMAP, Entekhabi et al., 2010) mission consists of a L-Band
294 radiometer at 1.4 Ghz with a mesh grid antenna (the radar component was only active during
295 the first 3 months of the mission). The National Snow and Ice Data Center Distributed Active
296 Archive Center (NSIDC DAAC, https://nsidc.org/data/smap) supplied a grid product
297 (SPL3SMP). The volumetric soil moisture obtained by the SMAP level 3 (version 4) passive
298 microwave radiometer, available from 2015 to the present, is included in this package. To match
299 the observations with the model grid space, the data for both SMOS and SMAP are resampled
300 to a 0.25◦ resolution in m^3/m^3. When more than one SM retrieval is available on a given day,
301 the daily average is employed to assure model time step consistency.

302 A drawback of our research is the comparison of model results assimilated with Soil Moisture
303 and Ocean Salinity (SMOS) data against other remote sensing observations, specifically from
304 the Soil Moisture Active Passive (SMAP) mission, instead of using in-situ data. While both
305 SMOS and SMAP provide valuable soil moisture information, they operate with different
306 sensing technologies and retrieval algorithms, leading to potential discrepancies in the observed

values. This methodological disparity can introduce biases and affect the accuracy of our model comparisons. Furthermore, the absence of in-situ data, which typically offers more precise and localized measurements, may limit the validation and robustness of our findings. By highlighting these considerations upfront, we aim to provide a clearer context for the interpretation of our results and underscore the necessity for caution when drawing conclusions based on these inter-comparisons.

3.2.4 Groundwater data

In-situ groundwater level data obtained from the Iran Water Resources Management Company (IWRMC) for observation wells distributed across the case study area (http://www.wrm.ir) is utilized. The size of each aquifer plays a crucial role in converting volumetric groundwater change values provided by IWRMC to equivalent water height. This conversion process is instrumental in ensuring a meaningful comparison. The results are then evaluated using an area-averaged time series of groundwater changes for each aquifer. Specifically, the modified in-situ groundwater time series, adjusted according to changes in well characteristics, seasonal variations, or calibration factors to address any biases or inaccuracies inherent in the initial measurements, are compared to the aquifer's average assimilation findings individually. This comparison provides insights into the effectiveness of the adjustments made to the in-situ groundwater time series in aligning it with the aquifer's average assimilation findings.

Table 1: List of used data including input data of ParFlow-CLM and evaluation dataset

		Resolution: Spatial / Temporal	**Data Source**	**Download Link or Reference**
Input Data	Atmospheric forcing	0.25°/ 3-hourly	GLDAS_NOAH	https://disc.gsfc.nasa.gov/datasets/GLDAS_NOAH025_3H_2.1
	Plant Functional Type	500 m/Yearly	MODIS satellite (land-use classification)	https://lpdaac.usgs.gov/products/mcd12q1v006/
	Soil Texture Data, Sand and Clay Percentage	-	FAO/UNESCO Digital Soil Map of the World	(Batjes, 1997)
	DEM	1 km	Global Multiresolution Terrain Elevation Data 2010	https://earthexplorer.usgs.gov/
	Manning's coefficient	-	Relationship between landcover type and manning's coefficient	(Asante et al., 2008)
Data Assimilation	GRACE TWS	1°/Monthly	CSR	https://www2.csr.utexas.edu/grace/RL05.html
	SMOS	25 Km/ Daily	CATDS	https://www.catds.fr
Evaluation Dataset	SMAP	36 Km/Daily	NSIDC DAAC/ SPL3SMP	https://nsidc.org/data/smap
	Groundwater	Point data/ Monthly	IWRMC	http://www.wrm.ir

3.3 Data assimilation framework

3.3.1 EnKF

The Ensemble Kalman Filter (EnKF) is widely used in the previous papers due to its flexibility and simplicity of use in land surface models (e.g., Draper et al., 2012; Crow and Wood, 2003). Model state ensembles are created for estimating error covariance matrix of the state variable. This allows optimal merging of observations and model prediction.

EnKF involves the computation of the updated state ensemble X_t^+ at time step t for the model-estimated state variable X_t which encompasses the saturation degree of all grids for each ensemble member i. It is worth noting that the Van Genuchten relationships define the correlation between the degree of saturation and pressure head. When the degree of saturation is updated, the pressure head is correspondingly updated as well.

$$X_t^{i+} = X_t^i + \mathbf{K_t}\left[L_t - \mathbf{H_t}X_t^i\right] \tag{6}$$

Here, the perturbed observation is L_t. Perturbed observation is SMOS and GRACE data for SM DA and GRACE DA, respectively. The Kalman gain K_t can be defined via:

$$\mathbf{K_t} = \mathbf{P_t}\mathbf{H_t^T}\left(\mathbf{R_t} + \mathbf{H_t}\mathbf{P_t}\mathbf{H_t^T}\right)^{-1} \tag{7}$$

Here, $\mathbf{R_t}$ is the observation error matrix (a priori assigned as the expected observation error of the soil moisture from SMOS or/and GRACE TWS data from GRACE, $\mathbf{H_t^T}$ is the operator matrix that maps observations to model states at time t (transposed), and $\mathbf{P_t}$ is the error covariance matrix for the state variable related to model prediction, which is obtained from:

$$\mathbf{P}_t = \frac{\sum_{i=1}^{N}\left(X_i - \bar{X}\right)\left(X_i - \bar{X}\right)^T}{N-1} \quad (8)$$

Here, $\bar{x}$ is the ensemble mean that contains values for all of the grid cells. The number of ensemble members is given by N. Similarly, $\mathbf{R_t}$ is computed as:

$$\mathbf{R}_t = \frac{\sum_{i=1}^{N}\left(L_i - \bar{L}\right)\left(L_i - \bar{L}\right)^T}{N-1} \quad (9)$$

where L stores the perturbed observations and $\bar{L}$ is the ensemble mean. The operator matrix that maps observations to model states can be computed as the following equations for SM DA scenario:

H=

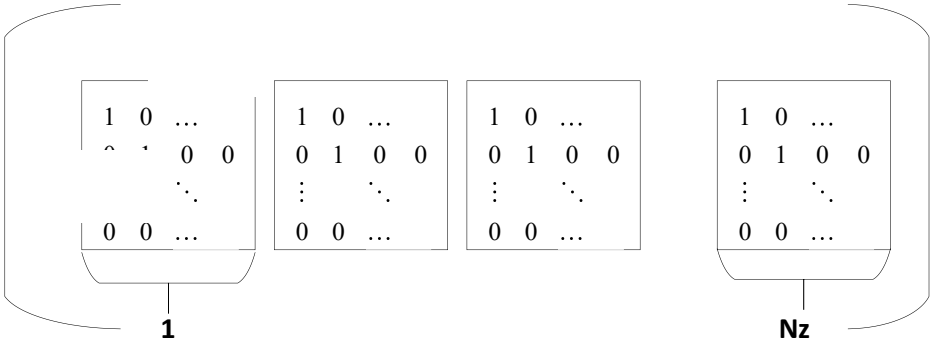

(10)

where L stores the perturbed observations and $\bar{L}$ is the ensemble mean. The operator matrix that maps observations to model states (**H**) is made by Eq. 4 and Eq. 5 for GRACE DA scenario. Data Assimilation Framework requires filter algorithm parameters, observation files, and instructions for building an ensemble of model runs as input (Figure 4). TWS/or SM data, it's error information was derived using GRACE level 2/or SMOS data, and generated ensembles of input data were obtained during pre-processing. Post-processing involves evaluating ParFlow-CLM output against independent data sets. We evaluated the results of simulations by a cross-validation with SMAP data and in-situ groundwater measurements as shown in Figure 4.

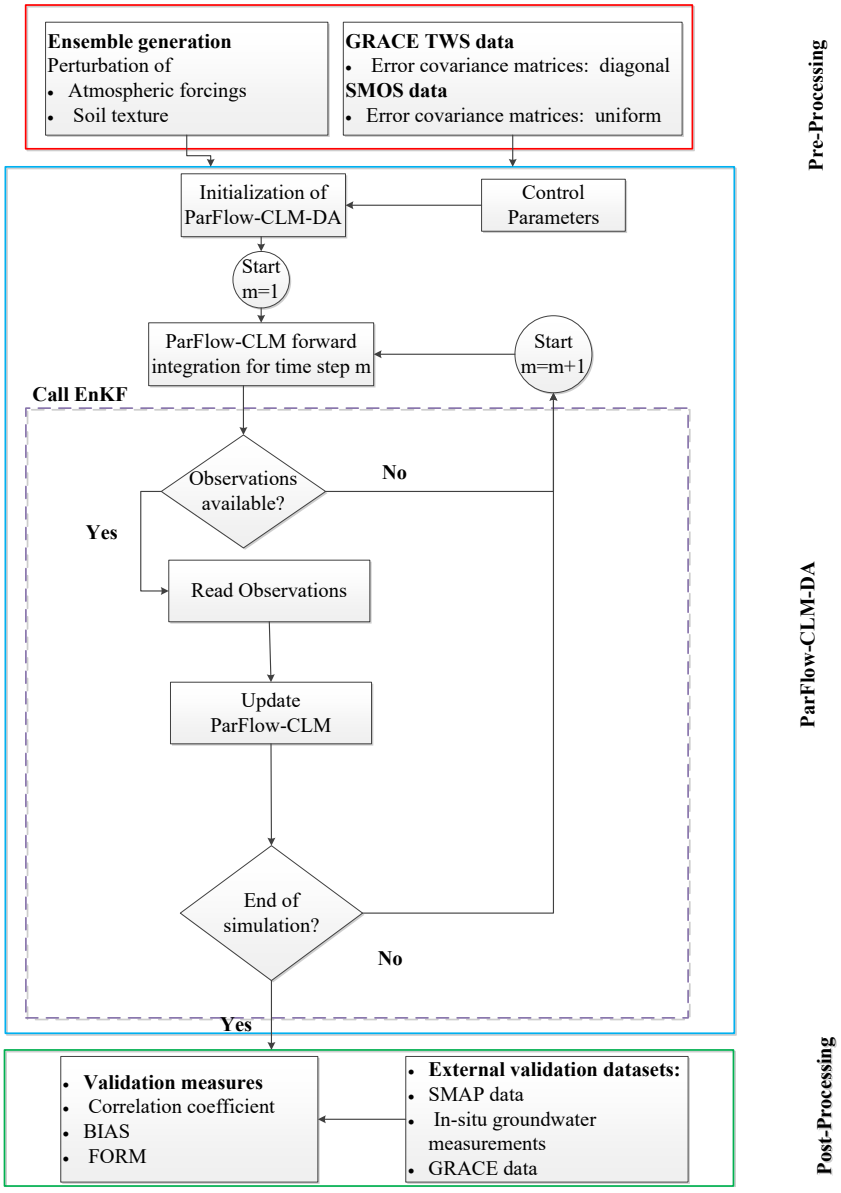

Figure 4. Flowchart showing the general set-up of the data assimilation including (i) the pre-processing of model input and observations, (ii) the data assimilation framework ParFlow-CLM-DA, and (iii) the post-processing to validate the DA performance.

3.3.2 ParFlow-CLM-DA experimental design

The assimilation tests were carried out from March 2015 to March 2020. To acquire equilibrium initial state variables, a ten-year spin up was undertaken by simulating the input data of 2015 ten times. We used ParFlow-CLM for a case study of Iran with a spatial resolution of 0.25° in this work. The model was run with a 3-hour time step (due to the temporal resolution of the GLDAS data) and a 5-day time window for soil moisture updates.

Because assimilation observations have various temporal resolutions, such as monthly GRACE TWS and daily soil moisture measurements, soil moisture observation is temporally rescaled into a 5-day resolution for data assimilation and GRACE TWS data is assimilated into the model in a monthly time scale. In this study, we assumed a spatially uniform observational error of 0.04 m^3/m^3 for SMOS (Colliander et al., 2017; Lievens et al., 2017) and a diagonal error covariance matrix for GRACE TWS data in the ParFlow-CLM-DA setup.

Both atmospheric forcing and soil properties affect the results of a land surface model. Precipitation and soil texture (%sand and %clay) were perturbed in this study to account for uncertainty in atmospheric forcing and soil texture. Precipitation received multiplicative perturbations that were log-normally distributed, geographically homogeneous, and temporally uncorrelated (Naz et al., 2019). The applied perturbation factors for precipitation had a mean and standard deviation of 1.0 and 0.10, respectively (Naz et al., 2019). A random noise with a standard deviation of 10% was used to perturb the sand and clay content (Naz et al., 2019). The

390 sand and clay content added up to 100%, in order to ensure the physical meaning of the soil
391 parameters. The sand and clay percentage have a direct impact on the computation of the soil
392 pedotransfer functions that links the hydraulic pressure in the soil to the water content of the
393 soil.

394 In the simulation/assimilation experiment, the initial ensemble size for precipitation and soil
395 texture was set to 36 to update the soil moisture of the top soil layer (0-15cm) and pressure
396 head. The main experiment consists of four ParFlow-CLM-DA simulations: (a) SMOS data
397 assimilation, (b) GRACE TWS data assimilation and (c) combined SMOS and GRACE data
398 assimilation, and (d) ensemble open-loop simulation (no data assimilation) (Figure 5).

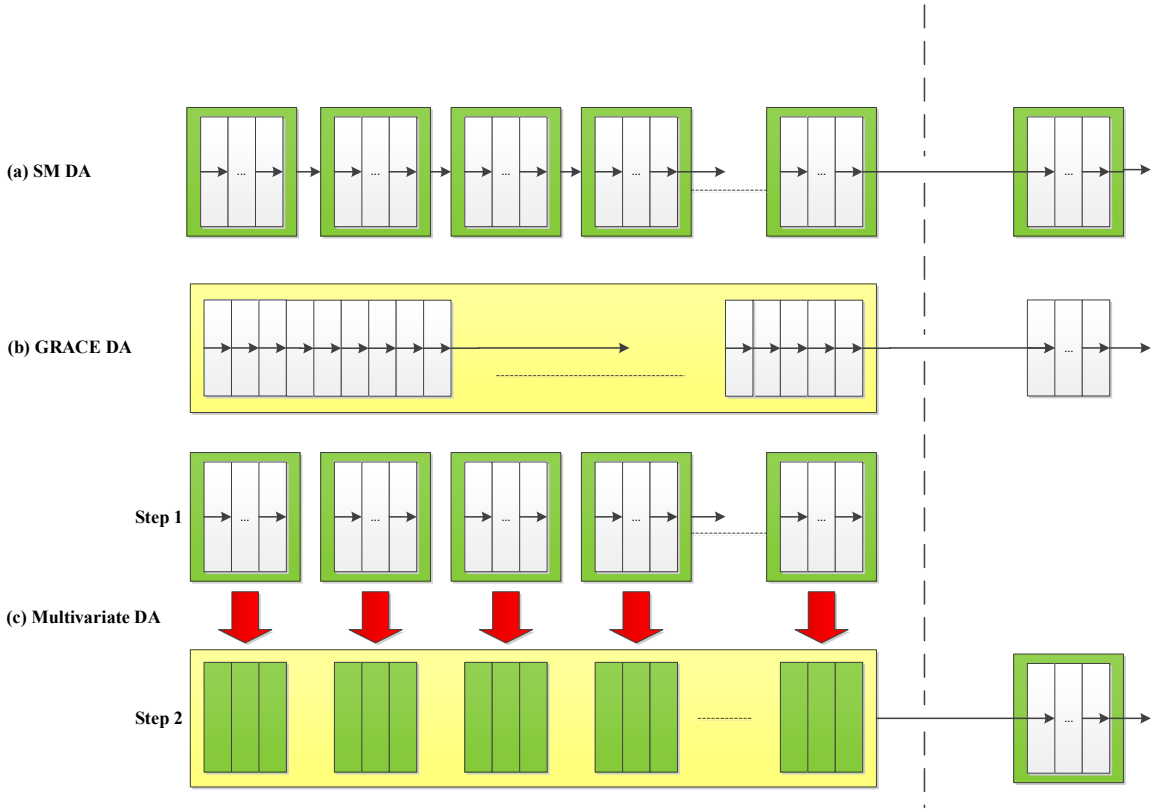

Figure 5. Three different DA scenarios, (a) SM DA, (b) GRACE DA, and (c) multivariate DA. The SM DA updates the state estimate using the time window of approximately five days (green rectangle in (a)) while the GRACE DA uses the time window of approximately one month (yellow rectangle in (b)). In the multivariate DA (c), the SM DA is first performed using the time window of approximately five days and its updated states are used as the forecast state in the GRACE DA using the time window of approximately one month.

3.4 Evaluation

3.4.1 Deterministic assessment

To assess model performance in simulating hydrological variables, we use absolute error, bias (BIAS), the correlation coefficient (R) and a probabilistic reliability assessment. These metrics are calculated as follows:

$$Absolute\,Error = \sum_{i=1}^{n} Y_i - Y_{obs,i} \tag{11}$$

$$BIAS = \frac{\sum_{i=1}^{n} \left(Y_i - Y_{obs,i}\right)}{\sum_{i=1}^{n} Y_{obs,i}} \tag{12}$$

$$R = \frac{\sum_{i=1}^{n} (Y_{obs,i} - \bar{Y}_{obs})(Y_i - \bar{Y})}{\sqrt{\sum_{i=1}^{n} (Y_{obs,i} - \bar{Y}_{obs})^2 \sum_{i=1}^{n} (Y_i - \bar{Y})^2}} \tag{13}$$

Where n is the total number of time steps; Y_i and $Y_{obs,i}$ represent the simulated ensemble mean and observation values at time step i, respectively.

3.4.2 Probabilistic assessment: the first order reliability method

The First Order Reliability Method (FORM) is a frequently used approach for assessing a system's structural reliability (Zhao et al., 2020). To approximate the failure function of the

examined system, the technique uses a Limit State Function (LSF) constructed via a Taylor expansion in Eq. (14) (Soltani et al., 2020).

$$G(y) = L(y) = G(y_m) + \nabla G(y_m)^T .(y - y_m) \tag{14}$$

where G(y) is the water budget closure failure function of a hydrologic system, L(y) is the LSF linearization, $y = (y_1, y_2, ..., y_n)$ is the vector of n variables in G(y) function, y_m is the expansion point, and ∇G is the first order gradient vector of G(y).

In this study, FORM is used to assess the accuracy of the different DA experiments. The failure function G(y) defined as follows:

$$G(y) = r_i = \frac{\left| \text{Model } Estimation_i - Observation_i \right|}{\frac{1}{n}\sum_{1}^{n} P_i} \tag{15}$$

where *i* is a pixel number, and *n* is the total number of months. Since many recent studies found out that the accuracy of different DA strategies is between 5% and 25% of corresponding average precipitation (Long et al., 2014, Sahoo et al., 2011). We considered that when r_i of hydrologic system is less than 0.2, the model's results from different DA strategies are satisfactory.

The strategy seeks to find a point y* which is called the most probable failure point by calculating the shortest distance between the origin and failure surface with the constraint

of $G(\mathrm{y}) \leq 0$. This shortest distance is called the reliability index $\beta = \left\| y^* \right\|$ (see Soltani et al. (2020) for point-by-point application forms of this strategy).

The failure probability of G(y) which means the accuracy of different DA strategies is lower than 20% of corresponding average precipitation, can be approximated using the reliability index β after it has been calculated as follows:

$$P_f = \Phi(-\beta) \tag{16}$$

P_f is the hydrologic system's failure probability and $\Phi(-\beta)$ is the standard normal variates cumulative distribution (Madsen et al., 2006). A smaller value of P_f corresponds to reduced uncertainty in the accuracy of various Data Assimilation strategies, showing heightened accuracy of the different DA experiment's reliability.

4 Results and Discussions

4.1 DA impacts on spatially averaged state variables

4.1.1 Soil moisture dynamics

The spatially averaged time series of the SM_{0-15cm} estimated from the model top layer open loop (running the model without DA) and all DA strategies are presented in Figure 6. The SMAP data is used for validation which shows that the application of data assimilation reduces misfits between the results and SMAP data compared to the open loop. The validation is carried

452 out in terms of correlation and absolute error, with the estimated values presented in Figure 7
453 and Figure 8, respectively. With an averaged correlation value of 0.67, ParFlow-CLM performs
454 well in the estimate of the SM $_{0–15cm}$ and gives good agreement with SMAP data at all sites (see
455 ensemble open loop in Figure 7). The SMOS assimilation also minimizes erroneous peaks of
456 the SM $_{0–15cm}$ estimate, such as in November 2018 (Figure 6) and May 2018 (Figure 6), resulting
457 in greater agreement with the SMAP data. Clearly, the SMOS data should be considered in the
458 DA process in order to retain the accuracy (in terms of agreement with the SMAP data) of the
459 SM $_{0–15cm}$ estimate in the case study. The SM DA and multivariate DA increase the correlation
460 value by 0.17 and 0.22, respectively (from 0.67 to 0.84 and 0.89). Since satellite SM observation
461 is employed in the SM DA and multivariate DA, an improved outcome is expected. The
462 GRACE DA, on the other hand, appears to have a negative impact on the SM $_{0–15cm}$ estimate
463 (see, Figures 7**Erreur ! Source du renvoi introuvable.** and 8). The GRACE DA reduces the
464 correlation by 0.08 when compared to the ensemble open loop. Poor performance is owing to
465 sensitivity of GRACE data to the signal associated with the top soil component. The results of
466 multivariate DA utilizing SMOS and GRACE data between March 2015 and June 2017 are
467 compared to SMAP data (Figure 6). The daily SM $_{0–15cm}$ estimations of SMOS assimilation
468 clearly show a greater agreement with SMAP data (comparing to the ensemble open loop) (see,
469 Figures 7 and 8). The hydrological model did not benefit from the limited improvement in the
470 hydrological model's estimation of surface soil moisture with GRACE assimilation can be
471 attributed to GRACE's coarse spatial and temporal resolution. Additionally, the GRACE signal

472 is not sufficiently sensitive to surface soil moisture variations, as it is more adept at capturing
473 large-scale changes in terrestrial water storage. These factors hinder the model's ability to
474 benefit from GRACE data for precise surface soil moisture predictions. However, it should be
475 mentioned that even though soil moisture data assimilation improves the estimates for the top
476 soil moisture, the accuracy for the whole water column may not necessarily increase.

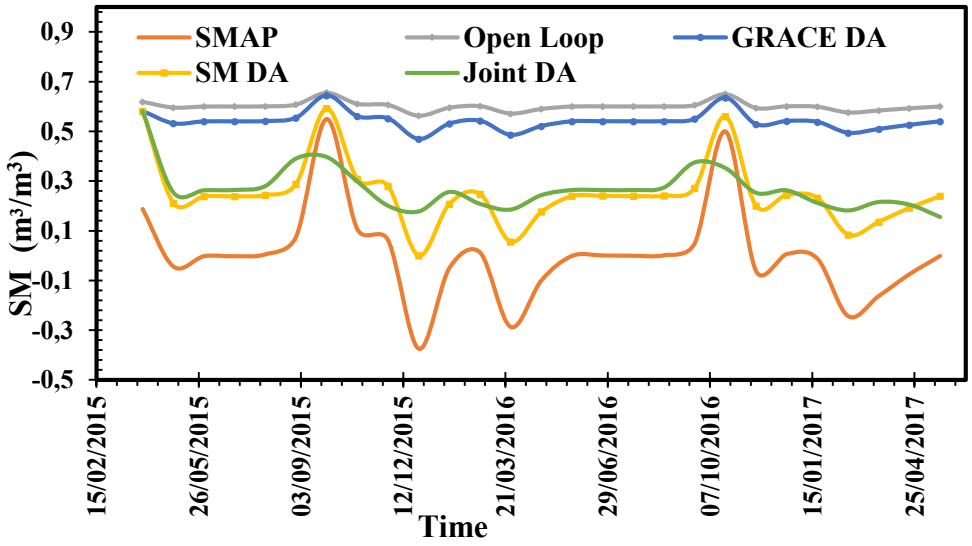

477

478 **Figure 6.** The monthly spatially averaged soil moisture (m^3/m^3) simulated for the first soil layer
479 (0-15 cm) using different DA strategies (SM DA, GRACE DA, and multivariate DA). The
480 SMAP observation and the ensemble open loop estimates are also shown for comparison.

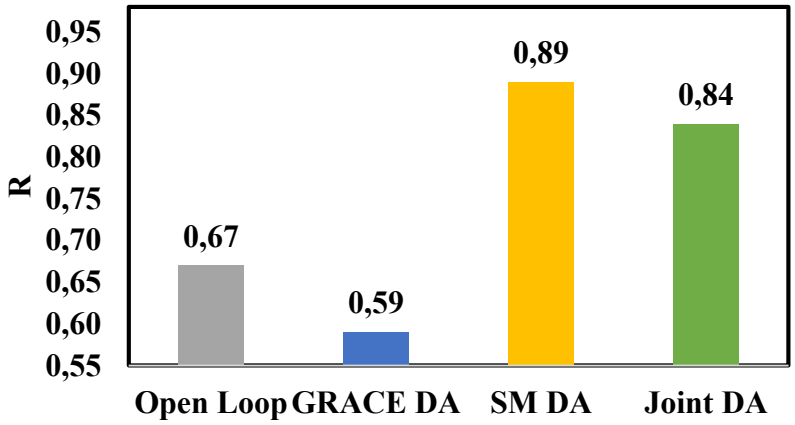

481

482 **Figure 7.** Averaged correlations between SM $_{0-15}$ cm variations derived using SMAP and
483 simulated by ParFlow-CLM before DA (open loop) using different DA strategies (SM DA,
484 GRACE DA, and joint DA)

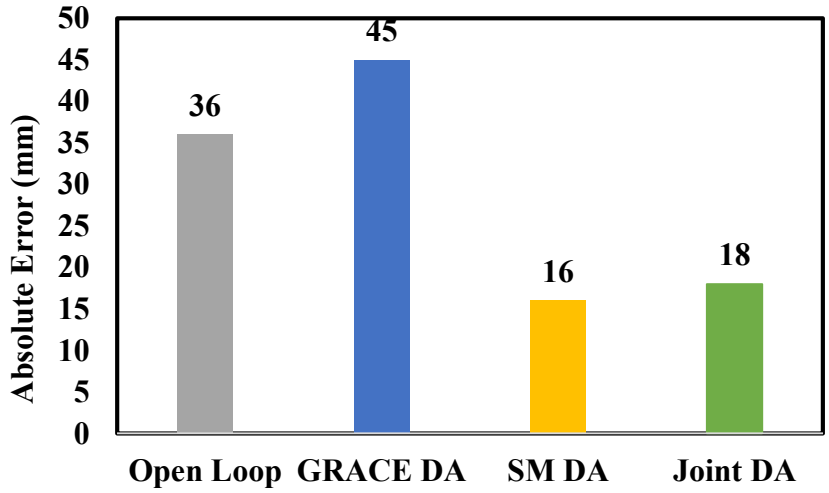

485

486 **Figure 8.** Absolute error of the SM $_{0-15\ cm}$ variations simulated by ParFlow-CLM before DA
487 (open loop) and using different DA strategies (SM DA, GRACE DA, and joint DA) when
488 compared with SMAP observations.

4.1.2 TWS variations

The basin-averaged time series of TWS variations from ParFlow-CLM before and after assimilating three different DA strategies is shown in Figure 9. It shows larger amplitude of TWS variations for the data assimilation results compared to open-loop results. Also, Figure 10, shows the correlation with respect to GRACE observations. Assimilating SM not only has the least impact on the TWS variations but also results in a negative impact on improving TWS estimates. The SM DA, reduces the averaged correlation value by ~0.07 (Figure 10). As a result, our findings show a lower level of agreement between the state estimate and the GRACE observation. SM assimilation appears to create a stimulatory effect that reduces the quality of TWS predictions.

In the GRACE DA, the improvement is applied to the entire water column, leading to an improved agreement between the TWS variation estimate and the GRACE observation. The averaged correlation value increase by 0.20 compared to open-loop results (Figure 10). GRACE DA appears to be more useful for improving TWS estimations than SM DA, but it may be of reduced benefit for the estimation of the other components (see, Figures 7 and 8). The idea of incorporating the SMOS and GRACE observations into the model at the same time is motivated by the underlying strengths of each individually.

Erreur ! Source du renvoi introuvable. Figure 9 also shows the multivariate DA results using SMOS and GRACE data between March 2015 and June 2017 when compared with GRACE

508 data. TWS estimations derived joint clearly demonstrate better agreement with GRACE data
509 (comparing to the ensemble open loop and GRACE DA). When compared to open-loop results,
510 the averaged correlation coefficient increases by 0.22 (Figure 10). The SM_{0-15cm} and TWS
511 variations components of the multivariate DA are modified toward the SMAP and GRACE
512 observations, yielding final state estimates that agree with both observations. TWS variations
513 predicted with multivariate DA agree with GRACE observations by 0.2 in cross-correlation
514 (Figure 10) while, at the same time, the SM_{0-15cm} estimate has a better correlation with SMAP
515 data by 0.17. (See Figure 7). TWS correlation increased by more than a factor of 1.3 using the
516 GRACE DA and multivariate DA (Figure 10). The SM DA, cannot provide a reliable TWS
517 estimate, as evidenced by the correlation, which is less than the GRACE DA and multivariate
518 DA (Figure 10).

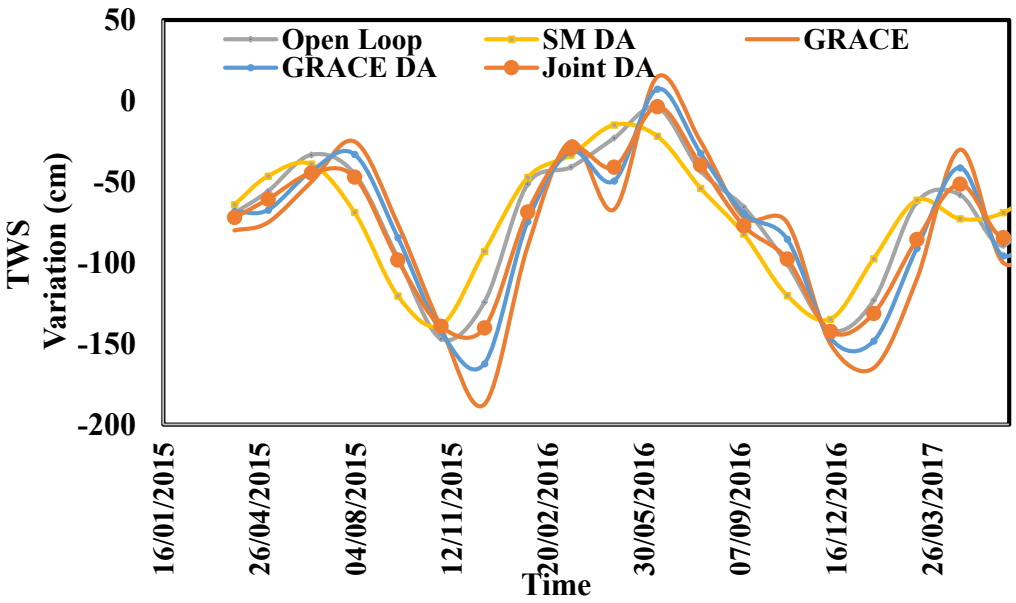

Figure 9. The monthly spatially averaged TWS variations (cm) simulated from different DA strategies (SM DA, GRACE DA, and multivariate DA). The GRACE observation and the ensemble open loop estimates are also shown for comparison.

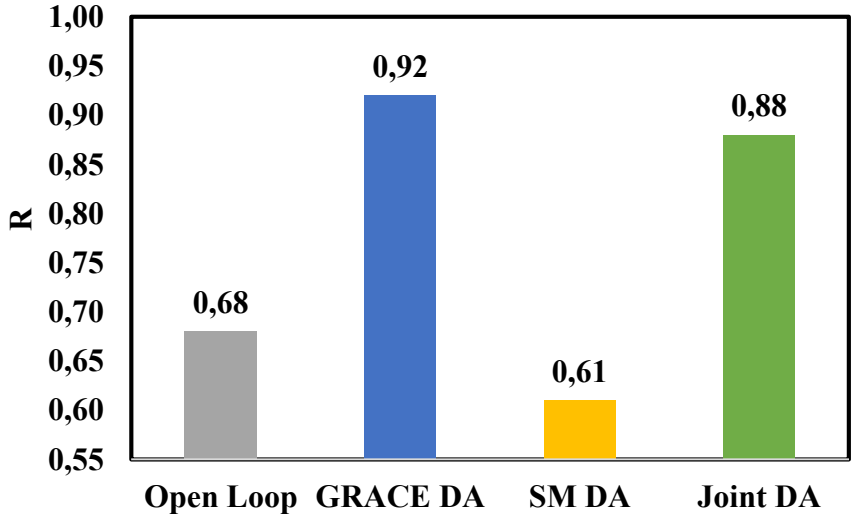

Figure 10. The average correlation coefficients (R) of the TWS variations simulated by different DA strategies (SM DA, GRACE DA, and multivariate DA) and the GRACE data.

4.1.3 Groundwater level variations

Figure 11 depicts the time series of monthly averaged groundwater (GW) level variations over the case study for the time period of 2015-2017. In-situ groundwater measurements are used to validate assimilation results of the different DA strategies. The average correlation coefficients and their absolute error in in-situ groundwater measurements are shown in Figures 12 and 13, respectively. The application of the SM DA results in inaccurate groundwater level estimates in Figure 12, with a considerable difference between the GW estimate and in-situ groundwater measurements. When compared to the ensemble open- loop estimate, the assimilation of GRACE data (in both GRACE DA and multivariate DA) boosts the correlation and reduces absolute error between the GW estimate and in-situ groundwater level changes by a factor of more than two (see, Figures 12 and 13). As a result, it is found that GRACE is more sensitive to the signal from the groundwater storage than the shallow storage component (similar to Tangdamrongsub et al. (2020)'s findings).

When compared to assimilating GRACE-only, assimilating both GRACE and SMOS observations performs better in the GW level variations estimate and delivers a 0.07 greater average correlation which is not a significant improvement (Figure 12). The GRACE DA updates GW level variations in the multivariate DA after the SM DA is applied. The use of the SM DA (in the multivariate DA) reduces the uncertainty of the state estimate, which increases the contribution of GRACE data in the GRACE DA. Groundwater trends are generally negative

551 over the entire time period (2015 – 2017). Again, it can be concluded that without using
552 assimilation, these correct negative trends are not captured.

553 Khaki et al. (2018b) integrated GRACE Total Water Storage (TWS) data into the World-Wide
554 Water Resources Assessment (W3RA) model, enabling a detailed examination of various water
555 budget components, including groundwater, soil moisture, and surface water storage, across
556 Iran's six major drainage divisions from 2002 to 2012. Their study revealed that assimilating
557 GRACE TWS data significantly enhances the W3RA model's performance, offering improved
558 insights into water availability in diverse locations. Particularly, the assimilation corrects for
559 open-loop simulation variations, a crucial aspect for accurate groundwater level estimation. Our
560 study, utilizing the ParFlow-CLM model, corroborates these findings, further supporting the
561 efficacy of GRACE TWS data assimilation in improving water resource assessments."

562 Khaki and Awange (2019) used the Ensemble Square-Root Filter (EnSRF) to integrate multi-
563 mission satellite datasets such as TWS from the GRACE satellite mission and soil moisture
564 products from the Advanced Microwave Scanning Radiometer-Earth Observing System
565 (AMSR-E) and SMOS into the W3RA model for estimating groundwater and soil moisture over
566 South America. The use of joint data assimilation improves W3RA estimations when compared
567 to groundwater in-situ measurements which is in a good agreement with our results. This effect
568 was clearly seen for TWS estimations and, more critically, groundwater simulations,

569 highlighting the potential for assimilating remotely sensed products to improve the W3RA
570 hydrological model's reliability.

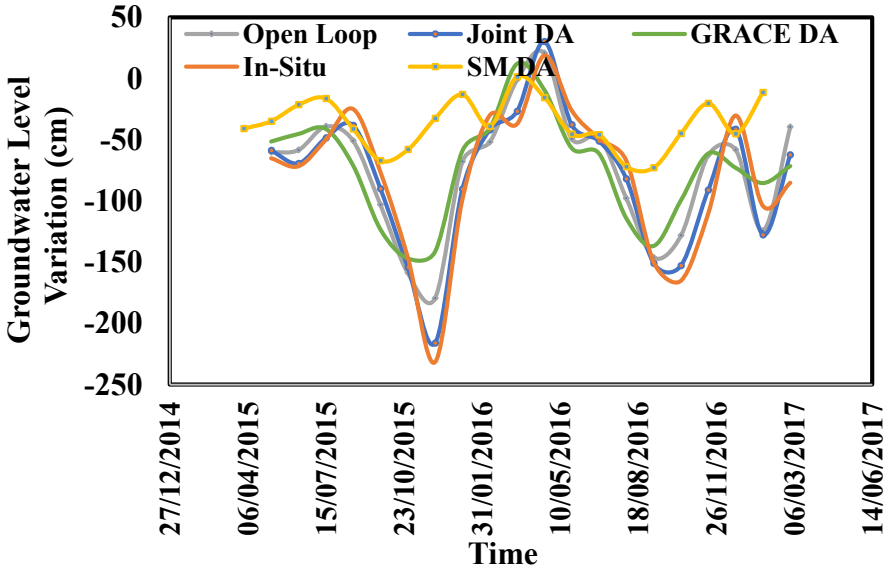

571

572 **Figure 11.** The monthly spatially averaged groundwater level variations (cm) simulated using
573 different DA strategies (SM DA, GRACE DA, and multivariate DA). The in-situ groundwater
574 measurements and the ensemble open-loop estimate are also shown for comparison.

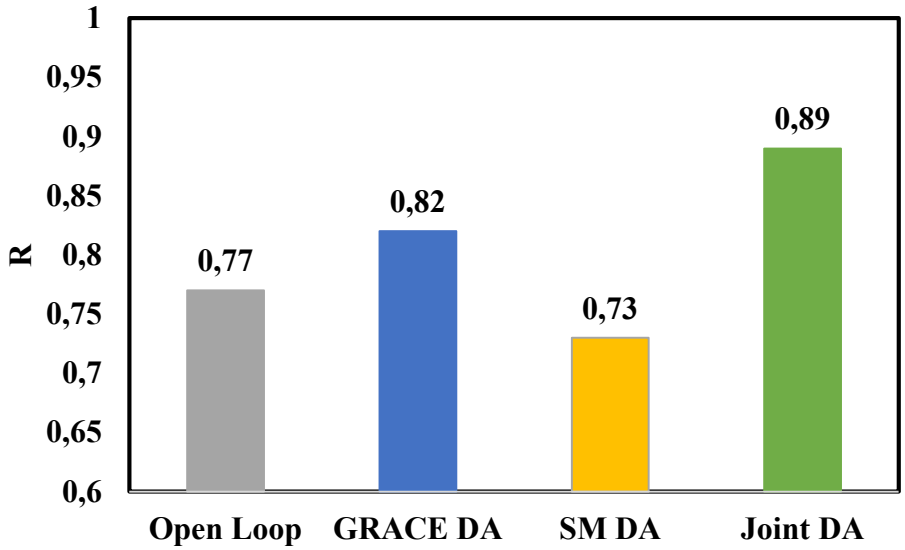

575

576 **Figure 12.** The Averaged correlation coefficients (R) of the groundwater level variations
577 simulated using different DA strategies (SM DA, GRACE DA, and multivariate DA) and in-
578 situ groundwater observations.

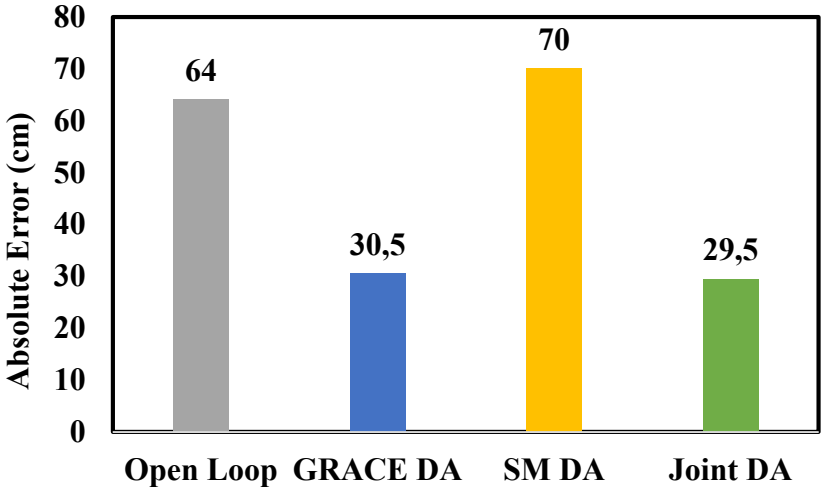

579

580 **Figure 13.** Absolute error for groundwater variations (cm) simulated by ParFlow-CLM before
581 DA (open loop) and after different DA strategies (SM DA, GRACE DA, and joint DA) when
582 compared to in-situ measurements.

583 **4.2 DA impacts on temporally averaged state variables**

584 Figure 14 shows temporally averaged SM_{0-15cm} variation from the ParFlow-CLM experiments
585 derived ensemble open loop and different DA strategies (SM DA, GRACE DA, and joint DA)
586 and the SMAP data over the time period of 2015-2017. Figure 15 evaluates the performance of
587 the DA in terms of BIAS error against the SMAP data to investigate the impact of different DA
588 strategies on the SM_{0-15cm} estimates. In comparison to the ensemble open loop, the SM DA
589 and multivariate DA provide smaller BIAS error values (Figure 15). This is to be expected,
590 given that the SMOS data are incorporated into the state estimate via the SM DA and
591 multivariate DA applications. The Kalman gain (Eq. 7) tries to statistically enhance the fit

between the SM_{0-15cm} estimates and the SMAP observation, resulting in better agreement (the maximum BIAS changes from 17.71 to 8.48).

GRACE DA, on the other hand, increases the BIAS error. The increase is most likely caused by low sensitivity of GRACE observations to top soil moisture. The top soil component is largely influenced by high-frequency meteorological forcing, but GRACE can only measure monthly basin-averaged TWS changes, which are dominated by deep-water storage component with low-frequency variability. GRACE data, with its coarse spatial and temporal resolution, faces challenges in accurately simulating the high spatiotemporal variability of water storage in the top soil layer. The satellite's measurements, covering large areas with intervals of several weeks to months, are insufficient for capturing the rapid and localized changes in the shallow top soil layer. As a result, GRACE alone may not provide the level of detail needed for precise modeling of water dynamics in this specific layer, highlighting the importance of complementing GRACE data with other sources or advanced modeling techniques. The BIAS error (ensemble spread) of the SM_{0-15cm} estimate is reduced in all DA strategies (Figure 15). The SM DA and multivariate DA reduce uncertainty when compared to the ensemble open loop, while the GRACE DA reduces uncertainty. Importantly, the SM DA and multivariate DA applications result in less uncertainty than the allocated SMAP uncertainty estimate.

Figure 16 evaluates the performance of the DA in terms of absolute error against the in-situ groundwater level measurements data to investigate the impact of different DA strategies on

611 the groundwater variation estimates. As shown in Figure 16, the BIAS inaccuracy indicates
612 bigger differences from north to south and the biggest BIAS error is evident in the southwest of
613 the basin. A similar pattern is seen in all DA scenarios. The BIAS inaccuracy in Figure 16
614 clearly demonstrates the effect of DA. In SM DA, the biggest uncertainty is seen compared to
615 other DA scenarios and ensemble open loop estimate, particularly in the central part of the
616 basin. In GRACE DA and joint DA, the uncertainty decreases, and the lowest uncertainty is
617 seen in the central part of the basin and this extends north and west when joint DA is employed.

618 Tangdamrongsub et al. (2020) assimilated multi-mission remote sensing observations,
619 including soil moisture information from SMOS and SMAP missions, as well as TWS
620 information from GRACE, into the Community Atmosphere and Biosphere Land Exchange
621 (CABLE) land surface model over the Goulburn River basin in Australia to enhance model
622 performance. The validation of data assimilation was conducted using in-situ soil moisture and
623 groundwater level data. The study revealed that SMOS assimilation improves topsoil moisture
624 but degrades groundwater level estimates. Conversely, GRACE assimilation enhances only the
625 groundwater component.

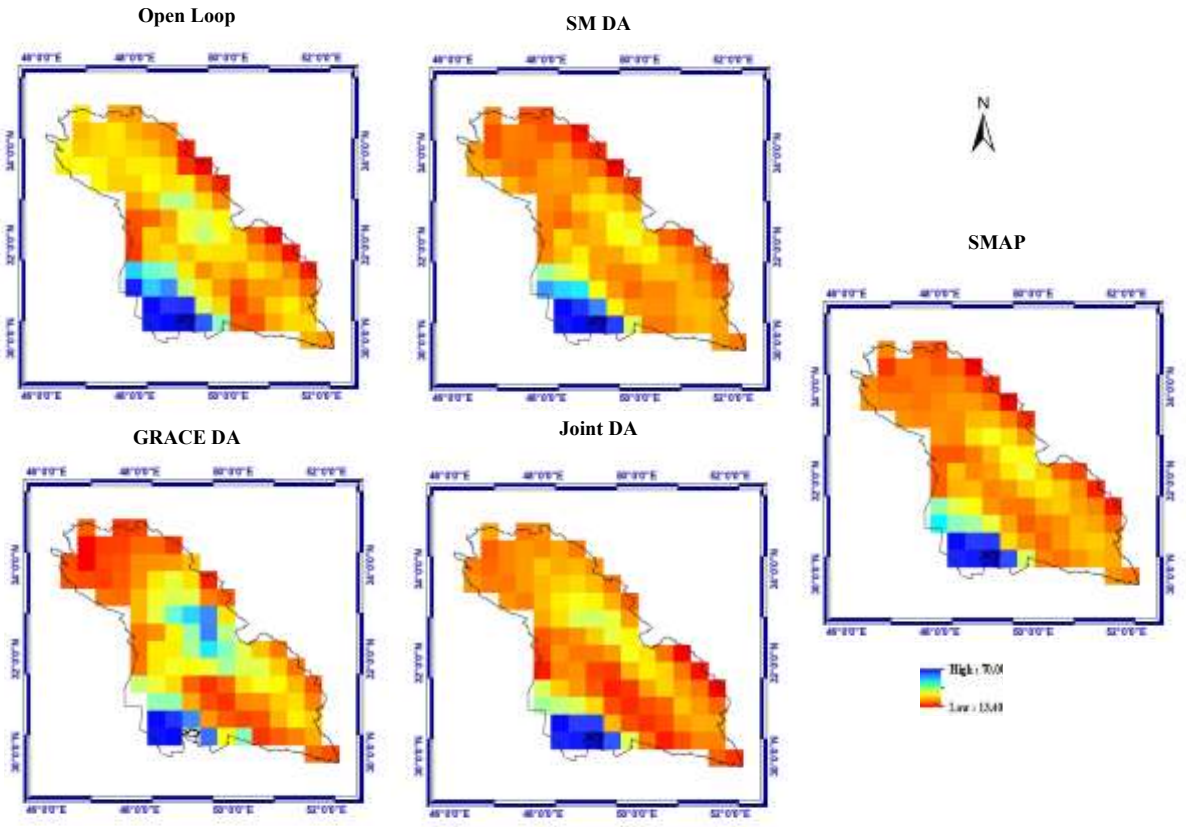

Figure 14. Temporally averaged soil moisture maps (mm) obtained using different DA strategies (SM DA, GRACE DA, and multivariate DA) over the case study. The ensemble open -loop estimates and SMAP data are also shown for comparison.

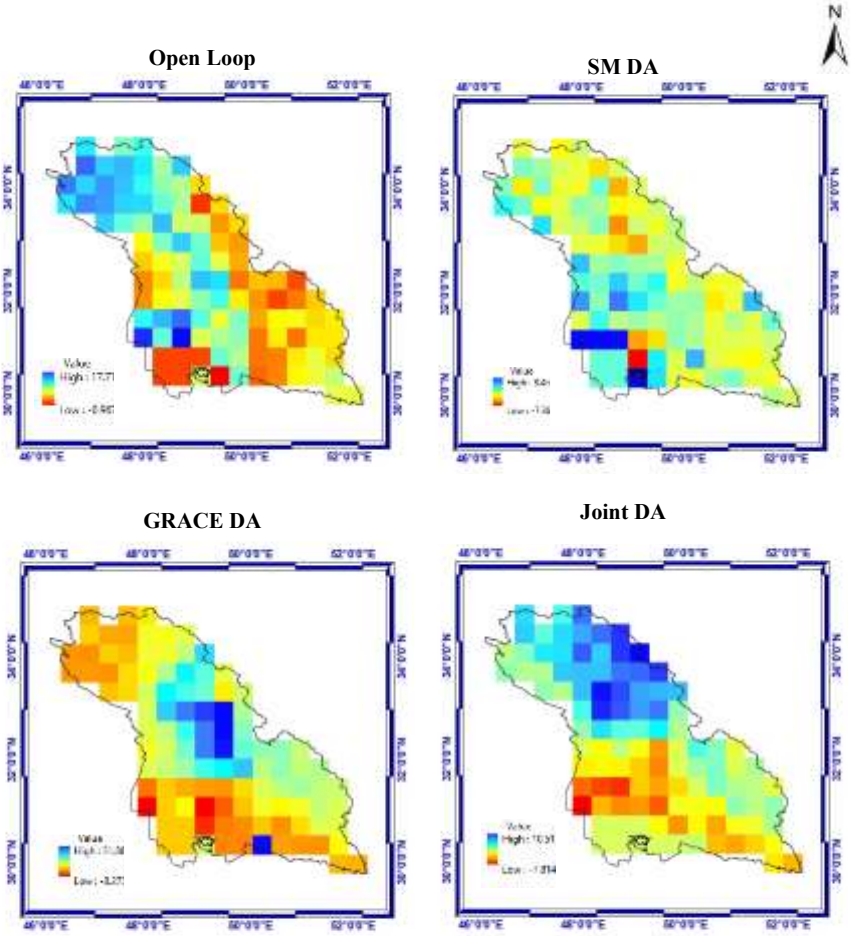

630

631 **Figure 15.** BIAS between temporally averaged soil moisture maps from different DA strategies
632 (SM DA, GRACE DA, and multivariate DA) and the SMAP data. The ensemble open-loop
633 estimate is also shown for comparison.

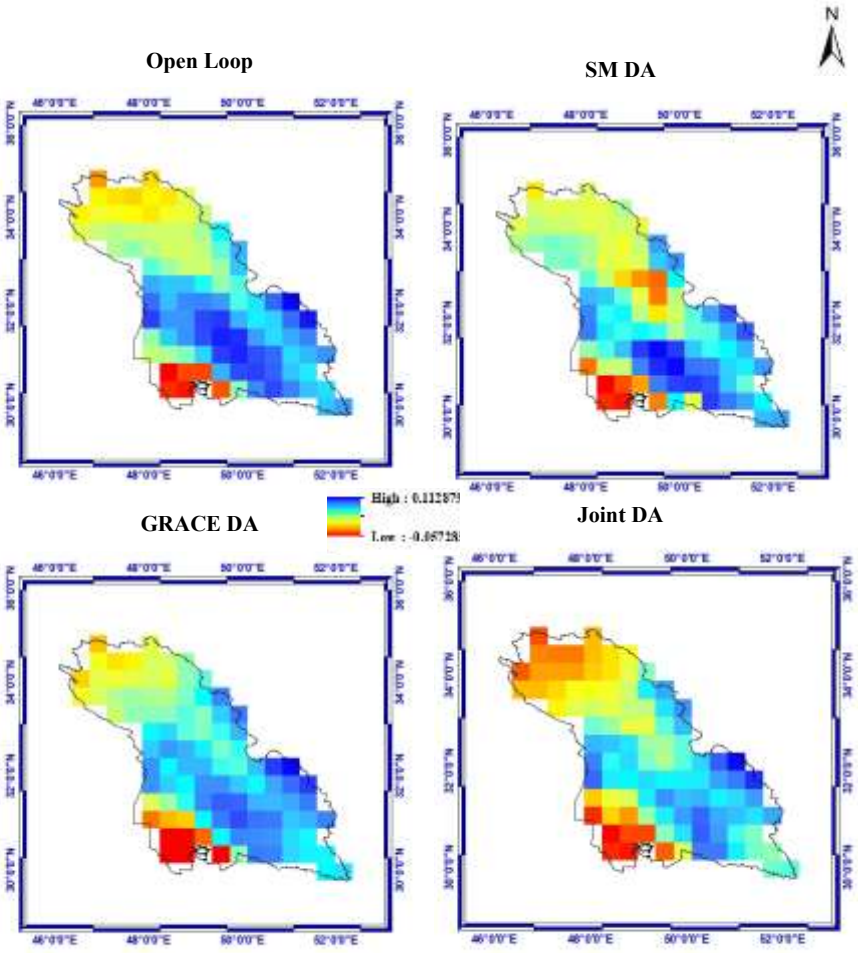

Figure 16. BIAS between temporally averaged groundwater level variations (cm) obtained using DA approaches (SM DA, GRACE DA, and multivariate DA) and in-situ groundwater level measurements.

4.3 Evaluating uncertainty in the DA strategies

The failure probability of LSF (refer to Eq.15) is investigated as a criterion to assess model reliability using a novel application of the First Order Reliability Method (FORM). Specifying

r smaller than 0.2 (see Section 3.4.2), can be used as a criterion to assess the reliability of model's results. To achieve this, the FORM calculates the failure probability (P_f) of the model's closure results. The results of the FORM implementation in **Table 2** show that failure probability of multivariate data assimilation has the lowest value, and the best solution was found to be multivariate data assimilation using both GRACE and SMOS data for improving soil moisture, TWS and groundwater estimates. P_f of groundwater estimate using SM DA is larger than all DA strategies, and P_f of groundwater estimate using GRACE DA and multivariate DA is lower than all DA strategies. P_f of TWS estimates using GRACE DA is lower than all DA strategies, and P_f of TWS estimates using SM DA is larger than all DA strategies. P_f of soil moisture estimate using SM DA is lower than all DA strategies, and P_f of soil moisture estimate using GRACE DA is larger than all DA strategies which indicates that the performance of DA mainly depends on the type of observations, the prediction variable of interest that are assimilate and the prediction variable of interest. Each DA strategy exhibits an acceptable P_f value; however, if one choice is to be made, the joint DA approach appears more promising. It has the potential to enhance both soil moisture and groundwater estimates. It is essential to note that the significance of this finding may vary depending on the chosen hydrological model under consideration and the states incorporated in the Ensemble Kalman filter.

659 **Table 2:** Evaluating uncertainty in the DA strategies and open-loop simulation

DA Strategies	P_f		
	Soil Moisture	Groundwater	TWS
Open Loop	13%	12%	12%
SM DA	7%	14%	14%
GRACE DA	15%	10%	5%
joint DA	9%	8%	7%

660

661 **5 Summary and conclusion**

662 In this pioneering study, a novel approach emerges as both soil moisture from SMOS and total
663 water storage (TWS) data from GRACE are concurrently assimilated into the coupled ParFlow-
664 CLM hydrology model. Significantly, this marks the first-time integration of data assimilation
665 (DA) techniques into the ParFlow-CLM model, a physically based model renowned for its
666 capability to capture intricate interactions between surface and subsurface water dynamics.

667 The intricacies of the interaction between subsurface and surface water are adeptly addressed
668 through the utilization of the coupled surface-subsurface ParFlow-CLM model. This model,
669 renowned for its physical realism, proves instrumental in simulating the complex processes
670 occurring at the interface between the deeper subsurface and the surface.

Three innovative data assimilation strategies are deployed to assimilate either one or both of GRACE and SMOS satellite products for basins in Iran. The assimilation method demonstrates proficiency in estimating soil moisture, particularly for the top 15 centimeters of the soil, when appropriate observations are incorporated. Strikingly, the assimilation of GRACE data significantly improves estimates of groundwater level variation, emphasizing its unique contribution.

The novel aspect of this work lies in the revelation that assimilating both GRACE and SMOS data results in more accurate soil moisture estimates. Notably, single observation assimilation proves crucial for achieving the highest accuracy. This underscores the importance of incorporating SMOS data for enhancing soil moisture assimilation and elevating its precision, resulting in a substantial increase in correlation coefficient with SMAP data.

In contrast to previous findings, the hydrological model in this study does not derive significant benefits from GRACE assimilation for estimating surface soil moisture values. The study acknowledges the well-documented uncertainties associated with total water storage, yet highlights the marginal impact of GRACE assimilation on reducing soil moisture uncertainty, cautioning against potential misattributions of deep groundwater to shallow groundwater.

The breakthrough solution identified in this study is the application of multivariate data assimilation for both GRACE and SMOS data. This innovative approach adjusts high and low frequency values through soil moisture and GRACE assimilation, respectively. Consequently,

690 the correlation coefficients for the top 15 centimeters of soil moisture and changes in
691 groundwater level experience substantial increases with SMAP data and in-situ measurements.

692 While multivariate data assimilation exhibits slightly lower performance compared to single
693 assimilations for their respective target zones, it represents a significant advancement in
694 improving soil moisture estimates. Importantly, the study underscores the utility of comparing
695 model results with SMAP data to assess the model's ability to replicate key aspects of satellite
696 observations, emphasizing the reliance on remotely sensed data in regions lacking in-situ
697 measurements.

698 The study's novelty is further accentuated by the integration of data assimilation into the
699 ParFlow-CLM model, a milestone that expands the model's capabilities and enhances its utility
700 in capturing the complexity of surface-subsurface interactions. Additionally, the proposed
701 generalization of multivariate data assimilation to various data sources represents a
702 groundbreaking step towards a more comprehensive and adaptable hydrological modeling
703 framework. To ensure the robustness of the assimilation process, the study highlights the need
704 for future investigations to conduct a cross-correlation analysis of SMOS errors, shedding light
705 on their patterns and quantifying their impact on the assimilation processes. Additionally,
706 despite the original resolution of GRACE exceeding 100 kilometers, the research demonstrates
707 its capacity to enhance groundwater level estimation accuracy for Iran at a 0.25° resolution,
708 presenting a noteworthy advancement in spatial resolution for groundwater studies.

We encourage future studies to utilize finer resolution data if available. This will likely enhance the precision of the simulations and address some of the drawbacks identified in our research. If higher-resolution atmospheric and surface datasets become accessible, we recommend repeating the simulations to potentially achieve more detailed and accurate results.

In addition to the points mentioned, it's important to note that the validation results of our ParFlow-CLM simulations should also be compared with those obtained from other data assimilation techniques. While our study focused on a specific approach, other techniques such as Particle Filter (PF), or variational methods could potentially offer different strengths and weaknesses in terms of accuracy and computational efficiency. These methods incorporate observational data in varied ways, which might enhance the simulation of surface soil moisture and other hydrological variables. Conducting comparative studies with these alternative techniques would provide a more comprehensive understanding of the relative performance and reliability of our results. This comparison could highlight the advantages of using a fully coupled model like ParFlow-CLM versus simpler or different data assimilation methods, offering valuable insights for future research and practical applications in hydrological modeling.

Declaration of competing interest

The authors do not have actual, perceived or potential conflicts of interest to declare.

Acknowledgements

The authors acknowledge the High-Performance Computing (HPC) Center at Sharif University of Technology for providing computational resources that have supported this research. Samira Soltani and Marwan Fahs would acknowledge the financial support from the scientific council of the National School of Water and Environmental Engineering of Strasbourg.

Appendix A: List of Abbreviations

Abbreviation	Meaning
CLM	**C**ommunity **L**and **M**odel
DA	**D**ata **A**ssimilation
EnKF	**En**semble **K**alman **F**ilter
FORM	**F**irst **O**rder **R**eliability **M**ethod
GRACE	**G**ravity **R**ecovery **a**nd **C**limate **E**xperiment
GW	**G**roundwater
IWRMC	**I**ran **W**ater **R**esources **M**anagement **C**ompany
LSF	**L**imit **S**tate **F**unction
ParFlow	**PAR**allel **FLOW**
SM	**S**oil **M**oisture
SMAP	**S**oil **M**oisture **A**ctive **P**assive
SMOS	**S**oil **M**oisture and **O**cean **S**alinity
TWSA	**T**errestrial **W**ater **S**torage **A**nomaly
W3RA	**W**orld-Wide **W**ater **R**esources **A**ssessment

733 **References**

734 Al Bitar, A., Mialon, A., Kerr, Y. H., Cabot, F., Richaume, P., Jacquette, E., Quesney, A.,
735 Mahmoodi, A., Tarot, S., and Parrens, M.: The global SMOS Level 3 daily soil moisture and
736 brightness temperature maps, Earth System Science Data, 9, 293-315, 2017.

737 Altaf, M., Butler, T., Mayo, T., Luo, X., Dawson, C., Heemink, A., and Hoteit, I.: A comparison
738 of ensemble Kalman filters for storm surge assimilation, Monthly Weather Review, 142, 2899-
739 2914, 2014.

740 Ardebili, S. M. S. and Khademalrasoul, A.: An analysis of liquid-biofuel production potential
741 from agricultural residues and animal fat (case study: Khuzestan Province), Journal of cleaner
742 production, 204, 819-831, 2018.

743 Asante, K. O., Artan, G. A., Pervez, S., Bandaragoda, C., and Verdin, J. P.: Technical manual
744 for the geospatial stream flow model (GeoSFM), World Wide Web, 605, 594-6151, 2008.

745 Ashby, S. F. and Falgout, R. D.: A parallel multigrid preconditioned conjugate gradient
746 algorithm for groundwater flow simulations, nuclear science and engineering, 124, 145-159,
747 1996.

748 Batjes, N.: A world dataset of derived soil properties by FAO–UNESCO soil unit for global
749 modelling, Soil use and management, 13, 9-16, 1997.

Bennett, A. F.: Inverse modeling of the ocean and atmosphere, Cambridge University Press2005.

Bertino, L., Evensen, G., and Wackernagel, H.: Sequential data assimilation techniques in oceanography, International Statistical Review, 71, 223-241, 2003.

Bettadpur, S.: Gravity recovery and climate experiment, Level-2 Gravity Field Product User Handbook (Rev. 3.0, May 29, 2012), GRACE, 327-734, 2012.

Bierkens, M. F. and Van den Hurk, B. J.: Groundwater convergence as a possible mechanism for multi-year persistence in rainfall, Geophysical Research Letters, 34, 2007.

Brodzik, M. J., Billingsley, B., Haran, T., Raup, B., and Savoie, M. H.: EASE-Grid 2.0: Incremental but significant improvements for Earth-gridded data sets, ISPRS International Journal of Geo-Information, 1, 32-45, 2012.

Chen, J., Li, J., Zhang, Z., and Ni, S.: Long-term groundwater variations in Northwest India from satellite gravity measurements, Global and Planetary Change, 116, 130-138, 2014.

Cheng, M. and Tapley, B. D.: Variations in the Earth's oblateness during the past 28 years, Journal of Geophysical Research: Solid Earth, 109, 2004.

Colliander, A., Jackson, T. J., Bindlish, R., Chan, S., Das, N., Kim, S., Cosh, M., Dunbar, R.,

766 Crow, W. T. and Wood, E. F.: The assimilation of remotely sensed soil brightness temperature
767 imagery into a land surface model using ensemble Kalman filtering: A case study based on
768 ESTAR measurements during SGP97, Advances in Water Resources, 26, 137-149, 2003.

769 Danielson, J. J. and Gesch, D. B.: Global multi-resolution terrain elevation data 2010
770 (GMTED2010), US Department of the Interior, US Geological Survey Washington, DC, USA,
771 2011.

772 Dillon, M. E., Skabar, Y. G., Ruiz, J., Kalnay, E., Collini, E. A., Echevarría, P., Saucedo, M.,
773 Miyoshi, T., and Kunii, M.: Application of the WRF-LETKF data assimilation system over
774 southern South America: Sensitivity to model physics, Weather and Forecasting, 31, 217-236,
775 2016.

776 Döll, P., Kaspar, F., and Lehner, B.: A global hydrological model for deriving water availability
777 indicators: model tuning and validation, Journal of Hydrology, 270, 105-134, 2003.

778 Dorigo, W., Hahn, S., Hohensinn, R., Paulik, C., Wagner, W., Drusch, M., and van Oevelen,
779 P.: The international soil moisture network-a data hosting facility for in situ soil moisture
780 measurements in support of SMOS cal/val, EGU General Assembly Conference Abstracts,
781 12063.

782 Draper, C., Reichle, R., De Lannoy, G., and Liu, Q.: Assimilation of passive and active
783 microwave soil moisture retrievals, Geophysical Research Letters, 39, 2012.

784 Entekhabi, D., Njoku, E. G., O'Neill, P. E., Kellogg, K. H., Crow, W. T., Edelstein, W. N.,
785 Entin, J. K., Goodman, S. D., Jackson, T. J., and Johnson, J.: The soil moisture active passive
786 (SMAP) mission, Proceedings of the IEEE, 98, 704-716, 2010.

787 Evensen, G.: The ensemble Kalman filter: Theoretical formulation and practical
788 implementation, Ocean dynamics, 53, 343-367, 2003.

789 Ferguson, I. M. and Maxwell, R. M.: Human impacts on terrestrial hydrology: climate change
790 versus pumping and irrigation, Environmental Research Letters, 7, 044022, 2012.

791 Friedl, M. A., McIver, D. K., Hodges, J. C., Zhang, X. Y., Muchoney, D., Strahler, A. H.,
792 Woodcock, C. E., Gopal, S., Schneider, A., and Cooper, A.: Global land cover mapping from
793 MODIS: algorithms and early results, Remote sensing of Environment, 83, 287-302, 2002.

794 Garner, T., Wolf, R., Spiro, R., and Thomsen, M.: First attempt at assimilating data to constrain
795 a magnetospheric model, Journal of Geophysical Research: Space Physics, 104, 25145-25152,
796 1999.

797 Green, T. R., Taniguchi, M., Kooi, H., Gurdak, J. J., Allen, D. M., Hiscock, K. M., Treidel, H.,
798 and Aureli, A.: Beneath the surface of global change: Impacts of climate change on
799 groundwater, Journal of Hydrology, 405, 532-560, 2011.

Hirschi, M.: S. Seneviratne, S. Hagemann, and C. Schär, 2007: Analysis of seasonal terrestrial water storage variations in regional climate simulations over Europe, J. Geophys. Res, 112, D22109, 2007.

Hoteit, I., Luo, X., and Pham, D.-T.: Particle Kalman filtering: A nonlinear Bayesian framework for ensemble Kalman filters, Monthly weather review, 140, 528-542, 2012.

Jamei, M., Mousavi Baygi, M., Oskouei, E. A., and Lopez-Baeza, E.: Validation of the SMOS level 1C brightness temperature and level 2 soil moisture data over the west and southwest of Iran, Remote Sensing, 12, 2819, 2020.

Jasinski, M. F., Borak, J. S., Kumar, S. V., Mocko, D. M., Peters-Lidard, C. D., Rodell, M., Rui, H., Beaudoing, H. K., Vollmer, B. E., and Arsenault, K. R.: NCA-LDAS: overview and analysis of hydrologic trends for the national climate assessment, Journal of hydrometeorology, 20, 1595-1617, 2019.

Kerr, Y. H., Waldteufel, P., Richaume, P., Wigneron, J. P., Ferrazzoli, P., Mahmoodi, A., Al Bitar, A., Cabot, F., Gruhier, C., and Juglea, S. E.: The SMOS soil moisture retrieval algorithm, IEEE transactions on geoscience and remote sensing, 50, 1384-1403, 2012.

Khaki, M. and Awange, J.: The application of multi-mission satellite data assimilation for studying water storage changes over South America, Science of the Total Environment, 647, 1557-1572, 2019.

818 Khaki, M., Ait-El-Fquih, B., Hoteit, I., Forootan, E., Awange, J., and Kuhn, M.: Unsupervised
819 ensemble Kalman filtering with an uncertain constraint for land hydrological data assimilation,
820 Journal of Hydrology, 564, 175-190, 2018a.

821 Khaki, M., Forootan, E., Kuhn, M., Awange, J., van Dijk, A. I., Schumacher, M., and Sharifi,
822 M. A.: Determining water storage depletion within Iran by assimilating GRACE data into the
823 W3RA hydrological model, Advances in Water Resources, 114, 1-18, 2018b.

824 Kiany, M. S. K., Masoodian, S. A., Balling Jr, R. C., and Montazeri, M.: Evaluation of the
825 TRMM 3B42 product for extreme precipitation analysis over southwestern Iran, Advances in
826 Space Research, 66, 2094-2112, 2020.

827 Kollet, S. J. and Maxwell, R. M.: Integrated surface–groundwater flow modeling: A free-
828 surface overland flow boundary condition in a parallel groundwater flow model, Advances in
829 Water Resources, 29, 945-958, 2006.

830 Kollet, S. J. and Maxwell, R. M.: Capturing the influence of groundwater dynamics on land
831 surface processes using an integrated, distributed watershed model, Water Resources Research,
832 44, 2008.

833 Koster, R. D., Mahanama, S., Yamada, T., Balsamo, G., Berg, A., Boisserie, M., Dirmeyer, P.,
834 Doblas-Reyes, F., Drewitt, G., and Gordon, C.: Contribution of land surface initialization to

subseasonal forecast skill: First results from a multi-model experiment, Geophysical Research Letters, 37, 2010.

Kourgialas, N. N. and Karatzas, G. P.: A modeling approach for agricultural water management in citrus orchards: cost-effective irrigation scheduling and agrochemical transport simulation, Environmental monitoring and assessment, 187, 1-21, 2015.

Kumar, S. V., Jasinski, M., Mocko, D. M., Rodell, M., Borak, J., Li, B., Beaudoing, H. K., and Peters-Lidard, C. D.: NCA-LDAS land analysis: Development and performance of a multisensor, multivariate land data assimilation system for the National Climate Assessment, Journal of Hydrometeorology, 20, 1571-1593, 2019.

Kurtz, W., He, G., Kollet, S. J., Maxwell, R. M., Vereecken, H., and Hendricks Franssen, H.-J.: TerrSysMP–PDAF (version 1.0): a modular high-performance data assimilation framework for an integrated land surface–subsurface model, Geoscientific Model Development, 9, 1341-1360, 2016.

Lahoz, W., Geer, A., Bekki, S., Bormann, N., Ceccherini, S., Elbern, H., Errera, Q., Eskes, H., Fonteyn, D., and Jackson, D.: The Assimilation of Envisat data (ASSET) project, Atmospheric Chemistry and Physics Discussions, 6, 12769-12824, 2006.

Li, B., Rodell, M., Zaitchik, B. F., Reichle, R. H., Koster, R. D., and van Dam, T. M.: Assimilation of GRACE terrestrial water storage into a land surface model: Evaluation and

potential value for drought monitoring in western and central Europe, Journal of Hydrology, 446, 103-115, 2012.

Lievens, H., Reichle, R. H., Liu, Q., De Lannoy, G. J., Dunbar, R. S., Kim, S., Das, N. N., Cosh, M., Walker, J. P., and Wagner, W.: Joint Sentinel-1 and SMAP data assimilation to improve soil moisture estimates, Geophysical research letters, 44, 6145-6153, 2017.

Long, D., Longuevergne, L., and Scanlon, B. R.: Uncertainty in evapotranspiration from land surface modeling, remote sensing, and GRACE satellites, Water Resources Research, 50, 1131-1151, 2014.

Madsen, H. O., Krenk, S., and Lind, N. C.: Methods of structural safety, Courier Corporation 2006.

Maxwell, R.M., Kollet, S.J., Smith, S.G., Woodward, C.S., Falgout, R.D. and Ferguson, I.M.: ParFlow User's Manual. Integrated Ground Water Modeling Center Report GWMI, 2016.

Naz, B. S., Kurtz, W., Montzka, C., Sharples, W., Goergen, K., Keune, J., Gao, H., Springer, A., Hendricks Franssen, H. J., and Kollet, S.: Improving soil moisture and runoff simulations at 3 km over Europe using land surface data assimilation, Hydrol. Earth Syst. Sci., 23, 277-301, 10.5194/hess-23-277-2019, 2019.

Oleson, K., Niu, G. Y., Yang, Z. L., Lawrence, D., Thornton, P., Lawrence, P., Stöckli, R., Dickinson, R., Bonan, G., and Levis, S.: Improvements to the Community Land Model and

871 their impact on the hydrological cycle, Journal of Geophysical Research: Biogeosciences, 113,
872 2008.

873 Oleson, K. W., Dai, Y., Bonan, G., Bosilovich, M., Dickinson, R., Dirmeyer, P., Hoffman, F.,
874 Houser, P., Levis, S., and Niu, G.-Y.: Technical description of the community land model
875 (CLM), Tech. Note NCAR/TN-461+ STR, 2004.

876 Rahmani, A.: Investigation of water management in Karun, Karkheh, and Zohreh-Jarahi basins
877 and its relationship with dust in Khuzestan, Iran Nature, 6, 111-131, 2021.

878 Raziei, T., Mofidi, A., Santos, J. A., and Bordi, I.: Spatial patterns and regimes of daily
879 precipitation in Iran in relation to large-scale atmospheric circulation, International Journal of
880 Climatology, 32, 1226-1237, 2012.

881 Sahoo, A. K., Pan, M., Troy, T. J., Vinukollu, R. K., Sheffield, J., and Wood, E. F.: Reconciling
882 the global terrestrial water budget using satellite remote sensing, Remote Sensing of
883 Environment, 115, 1850-1865, 2011.

884 Schaap, M. G. and Leij, F. J.: Database-related accuracy and uncertainty of pedotransfer
885 functions, Soil Science, 163, 765-779, 1998.

886 Schunk, R. W., Scherliess, L., Sojka, J. J., and Thompson, D. C.: USU global ionospheric data
887 assimilation models, Atmospheric and Environmental Remote Sensing Data Processing and
888 Utilization: an End-to-End System Perspective, 327-336, 2004.

889 Seneviratne, S. I., Corti, T., Davin, E. L., Hirschi, M., Jaeger, E. B., Lehner, I., Orlowsky, B.,
890 and Teuling, A. J.: Investigating soil moisture–climate interactions in a changing climate: A
891 review, Earth-Science Reviews, 99, 125-161, 2010.

892 Shrestha, P., Sulis, M., Masbou, M., Kollet, S., and Simmer, C.: A scale-consistent terrestrial
893 systems modeling platform based on COSMO, CLM, and ParFlow, Monthly weather review,
894 142, 3466-3483, 2014.

895 Soltani, S. S., Ataie-Ashtiani, B., and Simmons, C. T.: Review of assimilating GRACE
896 terrestrial water storage data into hydrological models: Advances, challenges and opportunities,
897 Earth-Science Reviews, 213, 103487, 2021.

898 Soltani, S. S., Ataie-Ashtiani, B., Danesh-Yazdi, M., and Simmons, C. T.: A probabilistic
899 framework for water budget estimation in low runoff regions: A case study of the central Basin
900 of Iran, Journal of Hydrology, 586, 124898, 2020.

901 Soltani, S. S.: Assimilating remote sensing information into a distributed hydrological model
902 for improving water budget predictions. Diss. Université de Strasbourg; Sharif University of
903 Technology (Tehran), 2022a.

904 Soltani, S. S., Fahs, M., Al Bitar, A., and Ataie-Ashtiani, B.: Improvement of soil moisture and
905 groundwater level estimations using a scale-consistent river parameterization for the coupled

ParFlow-CLM hydrological model: A case study of the Upper Rhine Basin, Journal of Hydrology, 610, 127991, 2022b.

Soltani, S. S., Fahs, M., Al Bitar, A., and Ataie-Ashtiani, B.: Fully coupled subsurface-land surface hydrological models: A scaling approach to improve subsurface storage predictions, Copernicus Meetings, 2022c.

Sulis, M., Williams, J. L., Shrestha, P., Diederich, M., Simmer, C., Kollet, S. J., and Maxwell, R. M.: Coupling groundwater, vegetation, and atmospheric processes: A comparison of two integrated models, Journal of Hydrometeorology, 18, 1489-1511, 2017.

Swenson, S. and Wahr, J.: Post-processing removal of correlated errors in GRACE data, Geophysical research letters, 33, 2006.

Swenson, S., Chambers, D., and Wahr, J.: Estimating geocenter variations from a combination of GRACE and ocean model output, Journal of Geophysical Research: Solid Earth, 113, 2008.

Tangdamrongsub, N., Steele-Dunne, S. C., Gunter, B. C., Ditmar, P. G., and Weerts, A. H.: Data assimilation of GRACE terrestrial water storage estimates into a regional hydrological model of the Rhine River basin, Hydrology and Earth System Sciences, 19, 2079-2100, 2015.

Tangdamrongsub, N., Han, S.-C., Yeo, I.-Y., Dong, J., Steele-Dunne, S. C., Willgoose, G., and Walker, J. P.: Multivariate data assimilation of GRACE, SMOS, SMAP measurements for

improved regional soil moisture and groundwater storage estimates, Advances in Water Resources, 135, 103477, 2020.

Tangdamrongsub, N., Steele-Dunne, S. C., Gunter, B. C., Ditmar, P. G., Sutanudjaja, E. H., Sun, Y., Xia, T., and Wang, Z.: Improving estimates of water resources in a semi-arid region by assimilating GRACE data into the PCR-GLOBWB hydrological model, Hydrology and Earth System Sciences, 21, 2053-2074, 2017.

Tian, S., Tregoning, P., Renzullo, L. J., van Dijk, A. I., Walker, J. P., Pauwels, V. R., and Allgeyer, S.: Improved water balance component estimates through joint assimilation of GRACE water storage and SMOS soil moisture retrievals, Water Resources Research, 53, 1820-1840, 2017.

Tapley, B. D., Bettadpur, S., Ries, J. C., Thompson, P. F., and Watkins, M. M.: GRACE measurements of mass variability in the Earth system, science, 305, 503-505, 2004.

Van Genuchten, M. T.: A closed-form equation for predicting the hydraulic conductivity of unsaturated soils, Soil science society of America journal, 44, 892-898, 1980.

Van den Hurk, B., Doblas-Reyes, F., Balsamo, G., Koster, R. D., Seneviratne, S. I., and Camargo, H.: Soil moisture effects on seasonal temperature and precipitation forecast scores in Europe, Climate dynamics, 38, 349-362, 2012.

940 Van Dijk, A. and Warren, G.: The Australian water resources assessment system, Version 0.5,
941 3, 2010.

942 Van Dijk, A., Renzullo, L. J., and Rodell, M.: Use of Gravity Recovery and Climate Experiment
943 terrestrial water storage retrievals to evaluate model estimates by the Australian water resources
944 assessment system, Water Resources Research, 47, 2011.

945 Vrugt, J. A., ter Braak, C. J., Diks, C. G., and Schoups, G.: Hydrologic data assimilation using
946 particle Markov chain Monte Carlo simulation: Theory, concepts and applications, Advances
947 in Water Resources, 51, 457-478, 2013.

948 Wahr, J., Molenaar, M., and Bryan, F.: Time variability of the Earth's gravity field:
949 Hydrological and oceanic effects and their possible detection using GRACE, Journal of
950 Geophysical Research: Solid Earth, 103, 30205-30229, 1998.

951 Yu, Y., Disse, M., Yu, R., Yu, G., Sun, L., Huttner, P., and Rumbaur, C.: Large-scale
952 hydrological modeling and decision-making for agricultural water consumption and allocation
953 in the main stem Tarim River, China, Water, 7, 2821-2839, 2015.

954 Zaitchik, B. F., Rodell, M., and Reichle, R. H.: Assimilation of GRACE terrestrial water storage
955 data into a land surface model: Results for the Mississippi River basin, Journal of
956 Hydrometeorology, 9, 535-548, 2008.

957 Zhao, W., Chen, Y., and Liu, J.: An effective first order reliability method based on Barzilai–
958 Borwein step, Applied Mathematical Modelling, 77, 1545-1563, 2020.